Dynamical mean-field theory and numerical renormalization group study of superconductivity in the attractive Hubbard model

J. Bauer,[1] A. C. Hewson,[2] and N. Dupuis[3]
[1]*Max-Planck Institute for Solid State Research, Heisenbergstr. 1, 70569 Stuttgart, Germany*
[2]*Department of Mathematics, Imperial College, London SW7 2AZ, United Kingdom*
[3]*Laboratoire de Physique Théorique de la Matière Condensée, Université Pierre et Marie Curie, CNRS-UMR 7600, 4 Place Jussieu, 75252 Paris Cedex 05, France*

(Received 15 January 2009; revised manuscript received 30 April 2009; published 16 June 2009)

We present a study of the attractive Hubbard model based on the dynamical mean-field theory (DMFT) combined with the numerical renormalization group (NRG). For this study, the NRG method is extended to deal with self-consistent solutions of effective impurity models with superconducting symmetry breaking. We give details of this extension and validate our calculations with DMFT results with antiferromagnetic ordering. We also present results for static and integrated quantities for different filling factors in the crossover from weak to strong-coupling superfluidity. We study the evolution of the single-particle spectra throughout the crossover regime. Although the DMFT does not include the interaction of the fermions with the Goldstone mode, we find strong deviations from the mean-field theory in the intermediate and strong-coupling regimes. In particular, we show that low-energy charge fluctuations induce a transfer of spectral weight from the Bogoliubov quasiparticles to a higher-energy incoherent hump.

DOI: 10.1103/PhysRevB.79.214518 PACS number(s): 71.10.Fd, 71.27.+a, 71.30.+h, 75.20.−g

I. INTRODUCTION

The Hubbard model of locally interacting fermions plays a fundamental role in the theory of condensed-matter physics and has become a standard model to study correlated electronic behavior. In its repulsive version depending on interaction strength and doping, it displays magnetic instabilities such as antiferromagnetism. However, there is also evidence[1–4] that there is a parameter range where it possesses a strong instability in the pairing channel to *d*-wave superconductivity (SC), which makes it a good candidate to describe many important aspects of the high-temperature superconductors. Its attractive counterpart (the model with an onsite pairing term) has a simpler phase diagram, as the ground state is an *s*-wave superconductor. At half filling, a degenerate charge-ordered state can also occur. For electrons in a solid, this model may seem inappropriate at first sight; but one can think of the local attraction between the electrons as mediated by a boson, for instance, a phonon or exciton, where any form of retardation is neglected.[5] Indeed, the Bardeen, Cooper, and Schrieffer[6] (BCS) theory for superconductivity uses a similar model with instantaneous local attraction albeit with an energy (Debye) cutoff. In ultracold atom experiments,[7] the interactions between the fermionic atoms in an optical trap can be tuned by a Feshbach resonance. For a broad resonance, there exists a regime where the effective interaction is well described by a local attraction. Superfluidity has been observed in such systems,[7–10] also in the case where the fermions are confined to an optical lattice.[11]

When tuning the interaction in models of attractive fermions, such as the attractive Hubbard model, one has two limiting cases: the weak-coupling BCS superfluidity and the strong-coupling Bose-Einstein condensation (BEC) of preformed pairs. The theoretical understanding which has been developed over the years is that the properties, such as the order parameter Δ_{sc} and the transition temperature T_c to the superfluid state, are connected by a smooth crossover, and approximate interpolation schemes between these limits have been devised.[12–15] Apart from its recent experimental realization for ultracold atoms in an optical trap,[7–10] there is experimental evidence that this BCS-BEC crossover has also relevance for strong-coupling and high-temperature superconductors. It has been claimed that these superconductors display properties in certain parts of the phase diagram, such as the pseudogap, that can be understood in terms of pairs preformed above the transition temperature T_c, in contrast to the BCS picture, where the pairs no longer exist above T_c.[5,16,17]

Many aspects of the attractive Hubbard model have already been investigated.[5,18] However, the dynamic response functions have received fairly little theoretical attention, and it is the predictions for these quantities through the crossover that will be the focus of the present paper. One particular question concerns the fermionic excitations in the one-particle spectral functions. These are dominated by sharp Bogoliubov excitations in the weak-coupling limit. However, at strong coupling, when the fermions are bound to pairs, we expect a decrease in the spectral weight carried by the Bogoliubov quasiparticles. In order to investigate in detail what happens throughout the crossover, a suitable approach to calculate dynamic quantities is required. In situations where the momentum dependence of the self-energy is not so important, such as in the Mott transition, the dynamical mean-field theory (DMFT) has proven to be useful as local interactions can be treated very accurately. A variety of methods such as perturbation theory, quantum Monte Carlo, as well as exact diagonalization (ED), and numerical renormalization group (NRG) are commonly used to solve the associated effective impurity model. Among these methods, the NRG is one of the more suitable ones to calculate low-temperature spectral functions. Since it was originally proposed by Wilson,[19] it

has been developed constantly over the years.[20] The way of calculating spectral functions has been given a solid basis by the recent approach[21,22] based on the complete basis set proposed by Anders and Schiller.[23] So far the NRG has, however, not been applied to self-consistent DMFT calculations with superconducting symmetry breaking. Here we will show in detail how the method can be extended to this situation and present results for the spectral functions. Some of the results have already been published in Ref. 24. DMFT studies for the attractive Hubbard model based on other "impurity solvers" have been carried out in the normal phase[25,26] and in the broken-symmetry phase.[16,27,28] There is also a recent study in two dimensions with cellular DMFT.[29]

Our paper is organized as follows. The model and DMFT-NRG approach are described in Sec. II. For this calculation, the DMFT-NRG approach has to be generalized to deal with the case of a superconducting bath. This generalization is described in detail in Sec. III. There is a mapping from the negative U model to the positive one when the lattice is bipartite. In the half-filled case, this mapping can be used to check the results for superconductivity with earlier DMFT-NRG calculations with antiferromagnetic (AFM) order. The mapping and comparison of the results is given in Sec. IV. In Sec. V we compare our results for static and integrated quantities, such as the anomalous expectation value or superfluid density, with results based on other approximations. Finally, in Sec. VI, we present results for dynamic response functions. We focus on the features in the one-electron spectral density. Dynamic susceptibilities calculated with the method described here have been reported in Ref. 24.

II. MODEL AND DMFT-NRG SETUP

The subject of this paper is a study of the attractive Hubbard model, which in the grand canonical formalism reads

$$H = \sum_{i,j,\sigma} (t_{ij} c^\dagger_{i,\sigma} c_{j,\sigma} + \text{H.c.}) - \mu \sum_{i\sigma} n_{i\sigma} - U \sum_i n_{i,\uparrow} n_{i,\downarrow}, \quad (1)$$

with the chemical potential μ, the interaction strength $U>0$, and the hopping parameters t_{ij}. $c^\dagger_{i,\sigma}$ creates a fermion at site i with spin σ and $n_{i,\sigma}=c^\dagger_{i,\sigma}c_{i,\sigma}$. The present calculations are confined to zero temperature; however, an extension to finite temperature is possible. To study superconducting order, we can include an explicit superconducting symmetry-breaking term,

$$H_{\text{sc}} = \Delta^0_{\text{sc}} \sum_{\boldsymbol{k}} [c^\dagger_{\boldsymbol{k},\uparrow} c^\dagger_{-\boldsymbol{k},\downarrow} + \text{H.c.}], \quad (2)$$

with an "external field" Δ^0_{sc}. In the superconducting case in Nambu space, the Green's function matrix is given by

$$\underline{G}_{\boldsymbol{k}}(\omega) = \begin{pmatrix} \langle\langle c_{\boldsymbol{k},\uparrow}; c^\dagger_{\boldsymbol{k},\uparrow}\rangle\rangle_\omega & \langle\langle c_{\boldsymbol{k},\uparrow}; c_{-\boldsymbol{k},\downarrow}\rangle\rangle_\omega \\ \langle\langle c^\dagger_{-\boldsymbol{k},\downarrow}; c^\dagger_{\boldsymbol{k},\uparrow}\rangle\rangle_\omega & \langle\langle c^\dagger_{-\boldsymbol{k},\downarrow}; c_{-\boldsymbol{k},\downarrow}\rangle\rangle_\omega \end{pmatrix}, \quad (3)$$

where we use the notation for the zero-temperature-retarded Green's functions for two operators A,B, $\langle\langle A;B\rangle\rangle_\omega := -i\int dt\,\theta(t) e^{i\omega t}\langle[A(t),B]\rangle$ with the expectation value in the ground state $\langle\ldots\rangle$. Upon including Eq. (2), the noninteracting Green's function matrix $\underline{G}^0_{\boldsymbol{k}}(\omega)$ has the form,

$$\underline{G}^0_{\boldsymbol{k}}(\omega)^{-1} = \begin{pmatrix} \omega - \xi_{\boldsymbol{k}} & \Delta^0_{\text{sc}} \\ \Delta^0_{\text{sc}} & \omega + \xi_{\boldsymbol{k}} \end{pmatrix}, \quad (4)$$

where $\xi_{\boldsymbol{k}}=\varepsilon_{\boldsymbol{k}}-\mu$. For the interacting system, we introduce the matrix self-energy $\underline{\Sigma}_{\boldsymbol{k}}(\omega)$ such that the inverse of the full Green's function matrix $\underline{G}_{\boldsymbol{k}}(\omega)$ is given by the Dyson equation

$$\underline{G}_{\boldsymbol{k}}(\omega)^{-1} = \underline{G}^0_{\boldsymbol{k}}(\omega)^{-1} - \underline{\Sigma}_{\boldsymbol{k}}(\omega). \quad (5)$$

We employ the dynamical mean-field theory to analyze the model (1). As effective impurity model, we consider the attractive Anderson impurity model in a superconducting medium,

$$H^{\text{sc}}_{\text{And}} = H_{\text{imp}} + \sum_{\boldsymbol{k},\sigma} \varepsilon_{\boldsymbol{k}} c^\dagger_{\boldsymbol{k},\sigma} c_{\boldsymbol{k},\sigma} + \sum_{\boldsymbol{k},\sigma} V_{\boldsymbol{k}} (c^\dagger_{\boldsymbol{k},\sigma} d_\sigma + \text{H.c.}) - \sum_{\boldsymbol{k}} \Delta_{\boldsymbol{k}} [c^\dagger_{\boldsymbol{k},\uparrow} c^\dagger_{-\boldsymbol{k},\downarrow} + c_{-\boldsymbol{k},\downarrow} c_{\boldsymbol{k},\uparrow}]. \quad (6)$$

where $H_{\text{imp}}=\Sigma_\sigma \varepsilon_d n_\sigma - U n_\uparrow n_\downarrow$ with $n_\sigma = d^\dagger_\sigma d_\sigma$ and d_σ is the fermionic operator on the impurity site. $\varepsilon_{\boldsymbol{k}}$, $V_{\boldsymbol{k}}$, and $\Delta_{\boldsymbol{k}}$ are parameters of the medium. For the model (6), the noninteracting Green's function matrix has the form,

$$\underline{G}_0(\omega)^{-1} = \omega \mathbb{1}_2 - \varepsilon_d \tau_3 - \underline{K}(\omega). \quad (7)$$

$\underline{K}(\omega)$ is the generalized matrix hybridization for the medium, with diagonal part

$$K_{11}(\omega) = \sum_{\boldsymbol{k}} V^2_{\boldsymbol{k}} \frac{\omega + \varepsilon_{\boldsymbol{k}}}{\omega^2 - (\varepsilon^2_{\boldsymbol{k}} + \Delta^2_{\boldsymbol{k}})}, \quad (8)$$

and off-diagonal part,

$$K_{21}(\omega) = \sum_{\boldsymbol{k}} V^2_{\boldsymbol{k}} \frac{\Delta_{\boldsymbol{k}}}{\omega^2 - (\varepsilon^2_{\boldsymbol{k}} + \Delta^2_{\boldsymbol{k}})}. \quad (9)$$

For a self-consistent NRG calculation of an effective impurity problem, one has to (i) calculate the effective impurity model parameters $V_{\boldsymbol{k}}$, $\varepsilon_{\boldsymbol{k}}$, and $\Delta_{\boldsymbol{k}}$ in Eq. (6) from a given input function $\underline{K}(\omega)$ and (ii) map Eq. (6) to the so-called linear-chain Hamiltonian, to which the iterative diagonalization of the NRG can be applied. Due to the symmetry breaking, the standard formulation[20] needs to be extended. The details of how this can be achieved are described in the next section.

In the case with superconducting symmetry breaking, the effective Weiss field is a 2×2 matrix $\underline{\mathcal{G}}^{-1}_0(t)$. The DMFT self-consistency equation in this case reads[30]

$$\underline{\mathcal{G}}^{-1}_0(\omega) = \underline{G}(\omega)^{-1} + \underline{\Sigma}(\omega), \quad (10)$$

with $\boldsymbol{k}$-independent self-energy.[31] Hence, we use the NRG to solve the effective impurity problem for a given medium $\underline{K}(\omega)$ and calculate $\underline{\Sigma}(\omega)$ as detailed in Appendix A 3. From this we can obtain the diagonal local lattice Green's function, which for the superconducting case takes the form

$$G(\omega) = \int d\varepsilon \frac{\rho_0(\varepsilon)(\zeta_2(\omega)+\varepsilon)}{[\zeta_1(\omega)-\varepsilon][\zeta_2(\omega)+\varepsilon]-\Sigma_{21}(\omega)\Sigma_{12}(\omega)}, \tag{11}$$

where $\rho_0(\varepsilon)$ is the density of states of the noninteracting fermions and $\zeta_1(\omega)=\omega+\mu-\Sigma_{11}(\omega)$ and $\zeta_2(\omega)=\omega-\mu-\Sigma_{22}(\omega)$. The off-diagonal part is given by

$$G^{\text{off}}(\omega) = \int d\varepsilon \frac{\rho_0(\varepsilon)\Sigma_{21}(\omega)}{[\zeta_1(\omega)-\varepsilon][\zeta_2(\omega)+\varepsilon]-\Sigma_{21}(\omega)\Sigma_{12}(\omega)}. \tag{12}$$

We denote $G_{11}=G$, $G_{21}=G^{\text{off}}$ and $G_{21}(\omega)=G_{12}(-\omega)^*$, and $G_{22}(\omega)=-G_{11}(-\omega)^*$. These Green's functions can be collected into the matrix $\underline{G}$. Having calculated the local Green's function $\underline{G}$, the self-consistency Eq. (10) determines the new effective Weiss field $\underline{\mathcal{G}}_0^{-1}(\omega)$. We take the impurity model in the form (6) and identify $\underline{G}_0(\omega)=\underline{\mathcal{G}}_0(\omega)$. Then from Eq. (7) we obtain an equation for the effective-medium matrix $\underline{K}(\omega)$. In the calculations with spontaneous superconducting order, we will always consider the limit $\Delta_{\text{sc}}^0 \to 0$ in Eq. (2), where a solution with superconducting symmetry breaking will have bath parameters $\Delta_k \neq 0$ in the effective impurity model (6). In Sec. IV we compare the results of our extended method with the ones from a well-known antiferromagnetic case in order to gauge the quality of the new scheme.

III. EXTENSION OF THE NRG FORMALISM WITH SUPERCONDUCTING SYMMETRY BREAKING

In this section, we give details for the extension of the DMFT-NRG calculations with superconducting symmetry breaking. We first outline how to extract the parameters of the impurity model from the medium function. Then we discuss the mapping to the linear-chain Hamiltonian with details in Appendix A 1. This is a generalization of the scheme for the normal case.[20] In Appendix A 3, we describe the generalization of the calculation of the self-energy via the higher-order Green's functions.

A. Parameters of the effective impurity model

In the self-consistent procedure, the parameters of the effective impurity model have to be determined from the input functions of the medium K_{11} and K_{21} [Eqs. (8) and (9)]. We start with the Hamiltonian in the form (6) and choose a discretization in the usual logarithmic way to intervals I_n^α, $I_n^+=(x_{n+1},x_n)$, $I_n^-=-(x_n,x_{n+1})$, and $x_n=x_0\Lambda^{-n}$ characterized by the parameter $\Lambda>1$ and x_0 is large enough to cover nonzero spectral weight. Following the normal discretization steps[20] retaining only the lowest Fourier component yields

$$H_{\text{And}}^{\text{sc}} = H_{\text{imp}} + \sum_{\sigma,n,\alpha} \xi_n^\alpha a_{\alpha,n,\sigma}^\dagger a_{\alpha,n,\sigma} + \sum_{\sigma,\alpha,n} \gamma_n^\alpha (a_{\alpha,n,\sigma}^\dagger d_\sigma + \text{H.c.}) - \sum_{\alpha,n} \delta_n^\alpha (a_{\alpha,n,\uparrow}^\dagger a_{\alpha,n,\downarrow}^\dagger + a_{\alpha,n,\downarrow} a_{\alpha,n,\uparrow}). \tag{13}$$

We outline a procedure to obtain the parameters ξ_n^α, γ_n^α, and δ_n^α. For the discretized model (13), we find similar equations to Eqs. (8) and (9),

$$K_{11}(z) = \sum_{n,\alpha} \gamma_n^{\alpha 2} \frac{z+\xi_n^\alpha}{z^2-E_n^{\alpha 2}}, \tag{14}$$

$$K_{21}(z) = \sum_{n,\alpha} \gamma_n^{\alpha 2} \frac{\delta_n^\alpha}{z^2-E_n^{\alpha 2}}, \tag{15}$$

with $E_n^\alpha=\sqrt{\xi_n^{\alpha 2}+\delta_n^{\alpha 2}}$. The imaginary parts $\Delta(\omega) := -\text{Im}\, K_{11}(\omega+i\eta)/\pi$ and $\Delta^{\text{off}}(\omega) := -\text{Im}\, K_{21}(\omega+i\eta)/\pi$ can be written as sums of delta functions,

$$\Delta(\omega) = \sum_{n,\alpha} \gamma_n^{\alpha 2} [u_{n,\alpha}^2 \delta(\omega - E_n^\alpha) + v_{n,\alpha}^2 \delta(\omega + E_n^\alpha)],$$

$$\Delta^{\text{off}}(\omega) = \sum_{n,\alpha} \gamma_n^{\alpha 2} u_{n,\alpha} v_{n,\alpha} [\delta(\omega - E_n^\alpha) - \delta(\omega + E_n^\alpha)],$$

where

$$u_{n,\alpha}^2 = \frac{1}{2}\left(1+\frac{\xi_n^\alpha}{E_n^\alpha}\right), \quad v_{n,\alpha}^2 = \frac{1}{2}\left(1-\frac{\xi_n^\alpha}{E_n^\alpha}\right), \tag{16}$$

with $u_{n,\alpha}^2+v_{n,\alpha}^2=1$. We define the spectral weights for the delta function representation in the intervals I_n^α by

$$w_{n,\alpha} = \int_{I_n^\alpha} d\omega \Delta(\omega), \quad \bar{w}_{n,\alpha} = \int_{I_n^\alpha} d\omega \Delta^{\text{off}}(\omega). \tag{17}$$

If we assume that $E_n^\alpha \in I_n^\alpha$ then the equations give for $\alpha=+$,

$$w_{n,+} = \gamma_n^{+2} u_{n,+}^2 + \gamma_n^{-2} u_{n,-}^2, \tag{18}$$

$$\bar{w}_{n,+} = \gamma_n^{+2} u_{n,+} v_{n,+} + \gamma_n^{-2} u_{n,-} v_{n,-}, \tag{19}$$

and similarly for $\alpha=-$. This leads to three independent equations to determine the four sets of independent parameters γ_n^{+2}, γ_n^{-2}, $u_{n,+}$, and $u_{n,-}$. Hence, we are free to choose one of them, e.g., $\gamma_n^{+2}=w_{n,+}$, from which follows directly $\gamma_n^{-2}=w_{n,-}$. We are then left with the equations

$$w_{n,+} - w_{n,-} = w_{n,+}(u_{n,+}^2 - v_{n,+}^2) + w_{n,-}(u_{n,-}^2 - v_{n,-}^2), \tag{20}$$

and

$$\bar{w}_{n,+} = w_{n,+} u_{n,+} v_{n,+} + w_{n,-} u_{n,-} v_{n,-}. \tag{21}$$

Using the equality

$$(u_{n,\alpha}^2 - v_{n,\alpha}^2)^2 = 1 - 4u_{n,\alpha}^2 v_{n,\alpha}^2, \tag{22}$$

we can derive a quadratic equation for $d_{uv,\alpha}=u_{n,\alpha}^2-v_{n,\alpha}^2$ with the solution

$$d_{uv,+} = [2\bar{w}_{n,+}^2(w_{n,+}^2 - w_{n,+}w_{n,-}) + w_{n,+}^4 + w_{n,+}w_{n,-} \times (w_{n,+}w_{n,-} - 2w_{n,+}^2) + 4\bar{w}_{n,+}^2 w_{n,+} \times \sqrt{w_{n,+}w_{n,-} - \bar{w}_{n,+}^2}]/[w_{n,+}w_{n,-}(w_{n,+}w_{n,-} - 2w_{n,+}^2) + w_{n,+}^4 + 4\bar{w}_{n,+}^2 w_{n,+}^2].$$

By definition, the parameters are then obtained from

$$\delta_n^\alpha = 2u_{n,\alpha}v_{n,\alpha}E_n^\alpha, \quad \xi_n^\alpha = (u_{n,\alpha}^2 - v_{n,\alpha}^2)E_n^\alpha. \tag{23}$$

In the symmetric case, $w_{n,+}=w_{n,-}$, this simplifies to

$$u_{n,+}^2 - v_{n,+}^2 = \sqrt{1 - \frac{\bar{w}_{n,+}^2}{w_{n,+}^2}}, \quad 2u_{n,+}v_{n,+} = \frac{\bar{w}_{n,+}}{w_{n,+}}. \tag{24}$$

such that

$$\delta_n^+ = \frac{\bar{w}_{n,+}}{w_{n,+}} E_n^+, \quad \delta_n^- = \frac{-\bar{w}_{n,-}}{w_{n,-}} E_n^-, \quad \xi_n^\alpha = \alpha \sqrt{1 - \frac{\bar{w}_{n,+}^2}{w_{n,+}^2}} E_n^\alpha.$$

Apart from the condition that it lies in the intervals I_n^α, E_n^α has not been specified, but it is reasonable to take a value in the middle of the intervals, i.e., $E_n^\alpha = |x_n + x_{n+1}|/2 > 0$. With this choice, all parameters are specified numerically and the discrete model is determined fully by the input functions. It can be easily checked that this procedure simplifies to the standard procedure[20] in the case without superconducting symmetry breaking.

It is also useful to check that in the case of a mean-field superconductor,[32–38] the usual expressions for the impurity parameters are recovered in this scheme. For simplicity, we assume $\Delta_{sc} \ll D$ in the following. Expression (A11) for the free impurity Green's function for this model yields for the medium functions analytically for $|\omega| > \Delta_{sc}$,

$$\Delta(\omega) = \frac{\Gamma}{\pi} \frac{|\omega|}{\sqrt{\omega^2 - \Delta_{sc}^2}} \tag{25}$$

and

$$\Delta^{\text{off}}(\omega) = \frac{\Gamma}{\pi} \frac{\Delta_{sc}}{\sqrt{\omega^2 - \Delta_{sc}^2}}. \tag{26}$$

With the described procedure, one finds apart from a small correction the standard results for ξ_n^α and γ_n^α. In addition, we obtain

$$\delta_n^\alpha \simeq \Delta_{sc}\left(1 + \frac{(\Lambda - 1)^2}{4} + \ldots\right) + \mathcal{O}(\Delta_{sc}^3), \tag{27}$$

where we used an expansion both in Δ_{sc} and $(\Lambda - 1)$. Hence, in the continuum limit, $\Lambda \to 1$, $\delta_n^\alpha = \Delta_{sc}$ comes out correctly as the constant mean-field gap parameter.

B. Mapping to the linear chain

The second important step (ii) in the self-consistent NRG procedure is to map the discretized model (13) to the so-called linear-chain model of the form,

$$H_{\text{And}} = H_{\text{imp}} + \sum_{\sigma,n=0}^{N} \varepsilon_n f_{n,\sigma}^\dagger f_{n,\sigma} + \sum_{\sigma,n=-1}^{N} \beta_n (f_{n,\sigma}^\dagger f_{n+1,\sigma} + \text{H.c.}) - \sum_{n=0}^{N} \Delta_n (f_{n,\uparrow}^\dagger f_{n,\downarrow}^\dagger + f_{n,\downarrow} f_{n,\uparrow}), \tag{28}$$

with $f_{-1,\sigma} = d_\sigma$ and $\beta_{-1} = \sqrt{\xi_0}$, with

$$\xi_0 = \sum_n (\gamma_n^{+2} + \gamma_n^{-2}). \tag{29}$$

As usual, we define the localized state

$$f_{0,\sigma} = \frac{1}{\sqrt{\xi_0}} \sum_n (\gamma_n^+ a_{+,n,\sigma} + \gamma_n^- a_{-,n,\sigma}). \tag{30}$$

The orthogonal transformation between the two Hamiltonians needs to be more general than in the standard case since with superconducting symmetry breaking we have superpositions of particles and holes in the medium. We choose the following ansatz for the transformation:

$$f_{n,\uparrow} = \sum_{\alpha,m} u_{\alpha,nm} a_{\alpha,m,\uparrow} - v_{\alpha,nm} a_{\alpha,m,\downarrow}^\dagger, \tag{31}$$

and

$$f_{n,\downarrow}^\dagger = \sum_{\alpha,m} v_{\alpha,nm} a_{\alpha,m,\uparrow} + u_{\alpha,nm} a_{\alpha,m,\downarrow}^\dagger. \tag{32}$$

We can now derive the recursion relations for the matrix elements and the parameters. This is done in generalization of the earlier work by Bulla *et al.*[39] and the details are given in Appendix A 1. We find for the parameters of the linear-chain Hamiltonian (28)

$$\varepsilon_n = \sum_{\alpha,m} \xi_m^\alpha (u_{\alpha,nm}^2 - v_{\alpha,nm}^2) + 2\delta_m^\alpha u_{\alpha,nm} v_{\alpha,nm}, \tag{33}$$

$$\Delta_n = \sum_{\alpha,m} \delta_n^\alpha (u_{\alpha,nm}^2 - v_{\alpha,nm}^2) - 2\xi_m^\alpha u_{\alpha,nm} v_{\alpha,nm}, \tag{34}$$

and

$$\beta_n^2 = \sum_{n',\alpha} \xi_{n'}^{\alpha 2} (u_{\alpha,nn'}^2 + v_{\alpha,nn'}^2) + \delta_{n'}^{\alpha 2} (u_{\alpha,nn'}^2 + v_{\alpha,nn'}^2) - \varepsilon_n^2 - \beta_{n-1}^2 - \Delta_n^2. \tag{35}$$

The recursion relations for the transformation matrix elements read as

$$\beta_n u_{\alpha,n+1n'} = (\xi_{n'}^\alpha - \varepsilon_n) u_{\alpha,nn'} + (\delta_{n'}^\alpha + \Delta_n) v_{\alpha,nn'} - \beta_{n-1} u_{\alpha,n-1n'} \tag{36}$$

and

$$\beta_n v_{\alpha,n+1n'} = (\delta_{n'}^\alpha - \Delta_n) u_{\alpha,nn'} - (\xi_{n'}^\alpha + \varepsilon_n) v_{\alpha,nn'} - \beta_{n-1} v_{\alpha,n-1n'}. \tag{37}$$

IV. COMPARISON WITH AFM-DMFT-NRG RESULTS

There is a canonical transformation which maps the attractive Hubbard model with arbitrary chemical potential to a half-filled repulsive model with a magnetic field,[5]

$$c_{i,\downarrow}^\dagger = e^{i\boldsymbol{q}_0 \boldsymbol{R}_i} b_{i,\downarrow}, \quad c_{i,\uparrow}^\dagger = b_{i,\uparrow}^\dagger,$$

$$c_{i,\downarrow} = e^{-i\boldsymbol{q}_0 \boldsymbol{R}_i} b_{i,\downarrow}^\dagger, \quad c_{i,\uparrow} = b_{i,\uparrow}, \tag{38}$$

with $\boldsymbol{q}_0$ such that $e^{i\boldsymbol{q}_0 \boldsymbol{R}_i}$ changes sign from one sublattice to another. At half filling, the respective states with broken symmetry, SC, and AFM orders correspond directly to each other. Hence, the quality of our method for the SC can be tested with well-known DMFT results from the case with AFM ordering.[40,41]

The mapping can be applied to map the corresponding effective impurity models of the two cases onto one another and we give the details in Appendix B. Here we use the mapping (38) to relate the dynamic response functions from the AFM and the SC cases, and we focus on the integrated spectral functions for the two calculations. In the antiferromagnetic case in the DMFT study, we usually use the A-B sublattice basis $C^{\dagger}_{\boldsymbol{k},\sigma}=(c^{\dagger}_{A,\boldsymbol{k},\sigma},c^{\dagger}_{B,\boldsymbol{k},\sigma})$,

$$G^{\mathrm{AFM}}_{\boldsymbol{k}}(\omega)=\begin{pmatrix}\langle\langle c_{A,\boldsymbol{k},\uparrow};c^{\dagger}_{A,\boldsymbol{k},\uparrow}\rangle\rangle_{\omega} & \langle\langle c_{A,\boldsymbol{k},\uparrow};c^{\dagger}_{B,\boldsymbol{k},\uparrow}\rangle\rangle_{\omega}\\ \langle\langle c_{B,\boldsymbol{k},\uparrow};c^{\dagger}_{A,\boldsymbol{k},\uparrow}\rangle\rangle_{\omega} & \langle\langle c_{B,\boldsymbol{k},\uparrow};c_{B,\boldsymbol{k},\uparrow}\rangle\rangle_{\omega}\end{pmatrix}. \quad (39)$$

where $\boldsymbol{k}$ is in the reduced Brillouin zone as we have doubled the Wigner-Seitz cell in position space including two lattice sites. The transformation from the attractive to the repulsive model (38) yields

$$c_{\boldsymbol{k},\uparrow}\rightarrow c_{A,\boldsymbol{k},\uparrow}+c_{B,\boldsymbol{k},\uparrow}, \quad (40)$$

$$c_{\boldsymbol{k},\downarrow}\rightarrow c^{\dagger}_{A,\boldsymbol{k},\uparrow}-c^{\dagger}_{B,\boldsymbol{k},\uparrow}. \quad (41)$$

Since we assume the Néel-type order, the quantities of the B lattice are related to the A-type lattice with opposite spin. We find

$$\langle\langle c_{\boldsymbol{k},\uparrow};c^{\dagger}_{\boldsymbol{k},\uparrow}\rangle\rangle_{\omega}\rightarrow G_{A,\boldsymbol{k},\uparrow,\uparrow}(\omega)+G_{A,\boldsymbol{k},\downarrow,\downarrow}(\omega)+G_{A,\boldsymbol{k},\uparrow,\downarrow}(\omega)+G_{A,\boldsymbol{k},\downarrow,\uparrow}(\omega).$$

The local lattice Green's function for the antiferromagnetic Green's function is obtained by $\boldsymbol{k}$ summation over the reduced Brillouin zone $\Sigma_{\boldsymbol{k}}\rightarrow\int d\varepsilon\rho_0(\varepsilon)/2$,

$$G_{A,\uparrow,\uparrow}(\omega)=\frac{1}{2}\int d\varepsilon\rho_0(\varepsilon)\frac{\zeta_{A,\downarrow}(\omega)}{\zeta_{A,\uparrow}(\omega)\zeta_{A,\downarrow}(\omega)-\varepsilon^2}, \quad (42)$$

where $\zeta_{\alpha,\sigma}(\omega)=\omega+\mu_{\sigma}-\Sigma_{\alpha,\sigma}(\omega)$. The off-diagonal elements vanish as product of a symmetric and antisymmetric function,

$$G_{A,\uparrow,\downarrow}(\omega)=\frac{1}{2}\int d\varepsilon\rho_0(\varepsilon)\frac{\varepsilon}{\zeta_{A,\uparrow}(\omega)\zeta_{A,\downarrow}(\omega)-\varepsilon^2}=0. \quad (43)$$

As a result, we can directly relate the diagonal local lattice Green's function $G_{11}(\omega)$ of the superconducting system to the sublattice Green's functions of the antiferromagnetic system,

$$G_{11}(\omega)=G_{A,\uparrow,\uparrow}(\omega)+G_{A,\downarrow,\downarrow}(\omega). \quad (44)$$

Similarly, one finds for the off-diagonal Green's function,

$$G_{12}(\omega)=G_{A,\uparrow,\uparrow}(\omega)-G_{A,\downarrow,\downarrow}(\omega). \quad (45)$$

The antiferromagnetic order parameter $\Delta_{\mathrm{AFM}}=Um_A$, $m_A=\frac{1}{2}(n_{A,\uparrow}-n_{A,\downarrow})$, is therefore directly related to the superconducting order parameter $\Delta_{\mathrm{sc}}=U\Phi$,

$$\Phi=\langle c_{0,\uparrow}c_{0,\downarrow}\rangle=\int_{-\infty}^{0}d\omega\left[-\frac{1}{\pi}\mathrm{Im}\,G^{\mathrm{off}}(\omega)\right]. \quad (46)$$

The results in this section are calculated with the Gaussian density of states $\rho_0(\varepsilon)=e^{-(\varepsilon/t^*)^2}/\sqrt{\pi}t^*$ corresponding to an infinite-dimensional hypercubic lattice. We define an effective bandwidth $W=2D$ for this density of states via the point at which $\rho_0(D)=\rho_0(0)/e^2$, giving $D=\sqrt{2}t^*$ corresponding to the choice in Ref. 42. We take the value $W=4$.

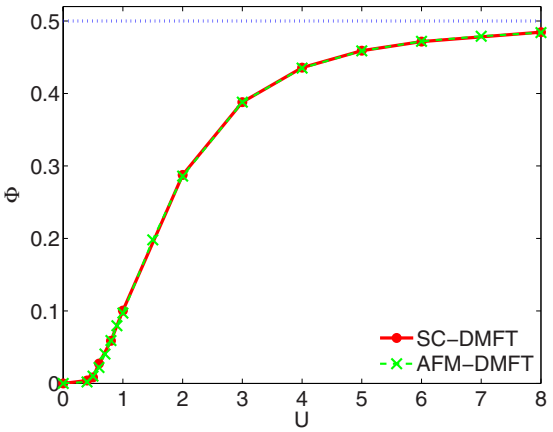

FIG. 1. (Color online) Comparison of the anomalous expectation value Φ in the attractive model with the local magnetization m_A in the AFM-DMFT calculations for half filling.

In Fig. 1, we show the comparison of the anomalous expectation value Φ (SC case) with the sublattice magnetization m_A (AFM case). We can see an excellent agreement of the corresponding expectation values from the two different calculations in all coupling regimes. In Fig. 2, we show the comparison for the Green's functions for $U=1,3,6$.

We can see that for the whole frequency range the overall agreement of these spectral functions is good. In the weak-coupling case $U=1$, differences can be seen in the height of the quasiparticle peaks, which are sharper and higher in the calculation with superconducting order. In contrast, at strong coupling $U=6$, the peaks are a bit broader and not as high as in the antiferromagnetic solution. It should be mentioned that for large U, DMFT-ED calculations in the AFM state have revealed spin polaron fine structure in the peaks.[43] These have so far escaped NRG calculations with less resolution at higher energy, but improved schemes might see this in the future. Generally, the results convey the picture of a good agreement for static and dynamic quantities for these two different DMFT-NRG calculations.

V. RESULTS FOR STATIC AND INTEGRATED QUANTITIES

Having tested the method at half filling, we discuss results for different filling factors in this section. We present results for static and integrated quantities obtained with the extended DMFT-NRG method. They can be compared to the quantities obtained with DMFT calculations with other impurity solvers such as iterated perturbation theory (IPT) (Ref. 27) or ED.[16] The semielliptic density of states with finite bandwidth $2D$ was used for all the following calculations:

$$\rho_0(\varepsilon)=\frac{2}{\pi D^2}\sqrt{D^2-\varepsilon^2}, \quad (47)$$

with $D=2t$ for the Hubbard model. $t=1$ sets the energy scale in the following. All the results presented here are for $T=0$. For many of the calculations, we take the model at quarter

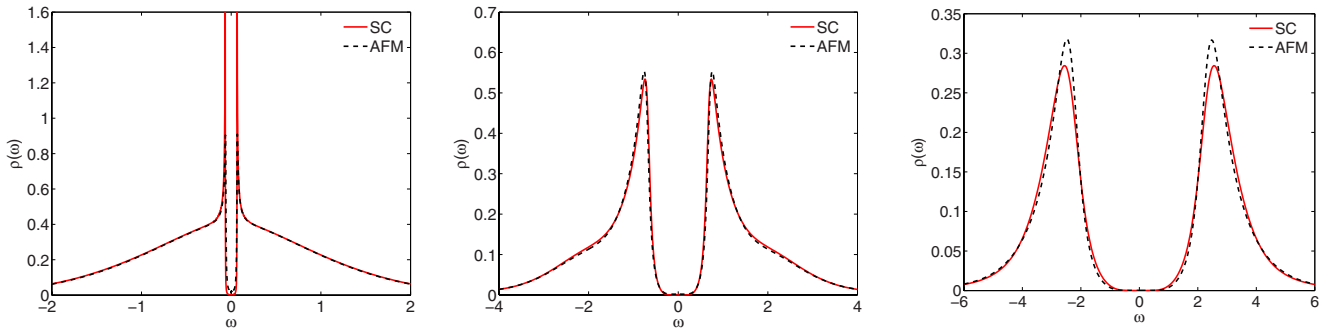

FIG. 2. (Color online) Comparison of the spectral functions of SC-DMFT and AFM-DMFT calculations for $U=1,3,6$ (left to right) for half filling.

filling ($n=1/2$) as a generic case to analyze. For the NRG calculations, we use $\Lambda=1.6$ and we keep 1000 states at each step. In the given units $U_c=2$ is the critical interaction for the bound-state formation in the two-body problem for the Bethe lattice[27] and can be referred to as unitarity in analogy to the crossover terminology of the continuum system.

A starting point for an analysis of many quantities in the BCS-BEC crossover in the attractive Hubbard model can be MF theory.[5] For a given U and filling factor n, the chemical potential μ_{MF} and the order parameter $\Delta_{\mathrm{sc,MF}}=U\Phi_{\mathrm{MF}}$ is determined by the mean-field equations. The fermionic excitations are given by $E_k^0=\sqrt{(\varepsilon_k-\bar{\mu})^2+\Delta_{\mathrm{sc,MF}}^2}$ with $\bar{\mu}=\mu_{\mathrm{MF}}+Un/2$. At weak coupling, the MF equations give the typical exponential behavior for Φ_{MF}, and for large U one finds

$$\mu_{\mathrm{MF}} \simeq -\frac{1}{2}U, \quad \Phi_{\mathrm{MF}} \simeq \frac{\sqrt{n(2-n)}}{2}. \tag{48}$$

If $\bar{\mu}$ is larger than the lower band energy (in our case $-D=-2$) then the minimal excitation energy is $\Delta_{\mathrm{sc,MF}}$ and occurs for $\varepsilon_k=\bar{\mu}$, which usually applies for weak coupling. For strong coupling and $n\simeq 1$, the minimal excitation energy is also given by $\Delta_{\mathrm{sc,MF}}$, which is on the order of U. However, for low density $n\to 0$, Eq. (48) yields $\bar{\mu}\to -U/2$, whereas Φ_{MF} and thus $\Delta_{\mathrm{sc,MF}}$ are small. Once $\bar{\mu}$ has become smaller than the lower band energy, the minimal excitation energy is still on the order of U as $E_{\mathrm{min}}^0=\sqrt{\bar{\mu}^2+\Delta_{\mathrm{sc,MF}}^2}=U$ independent of n. In the low-density strong-coupling limit, the excitation gap is given by $\bar{\mu}$ which then corresponds to the energy of the two-fermion bound state.

The mean-field spectral densities are given by

$$\rho_k^{\mathrm{MF}}(\omega) = u_k^2\delta(\omega-E_k^0)+v_k^2\delta(\omega+E_k^0), \tag{49}$$

$$\rho_k^{\mathrm{MF,off}}(\omega) = u_k v_k[\delta(\omega-E_k^0)-\delta(\omega+E_k^0)], \tag{50}$$

where $u_k^2=[1+(\varepsilon_k-\bar{\mu})/E_k^0]/2$, $v_k^2=1-u_k^2$. There are two bands of quasiparticle excitations given by $\pm E_k^0$, with weights u_k^2 for particle-like and v_k^2 for the hole-like excitations with infinite lifetime.

A. Behavior of the chemical potential

In Fig. 3, we plot our DMFT results for the chemical potential μ as a function of U for different densities n.

We can see that in all cases, the values tend to the mean-field value of $-U/2$ for large U. The results are in agreement with the ones reported by Garg *et al.*[27] and as seen there also to the MF values, which we did not include in the figure.

In the inset we show the quantity $\mu-Un/2$, which corresponds to $\bar{\mu}$ in the mean-field theory. When the density is low, e.g., $n=0.15$, it is seen to intersect with the lower band edge -2 at intermediate interactions $U\simeq 3.6$. Hence, μ plays a role to determine the fermionic excitation spectrum as discussed before. If its value does not change much with temperature and $\mu-Un/2$ remains smaller than $-D$ then no Fermi surface exists above T_c and the system does not possess fermionic character anymore as fermions are bound to composite pairs also above T_c. For large U, $\mu\sim -U/2$ gives the binding energy.

B. Anomalous expectation value

One of the characteristic quantities of the superconducting state is the presence of a finite anomalous expectation value Φ. In MF theory Φ increases exponentially at weak coupling. At strong coupling it only depends on the density n as seen in Eq. (48). In the attractive Hubbard model, the T_c increases exponentially with U and then decreases at strong coupling with t^2/U due to the kinetic term for hopping of fermionic pairs. This is captured in the DMFT calculation,

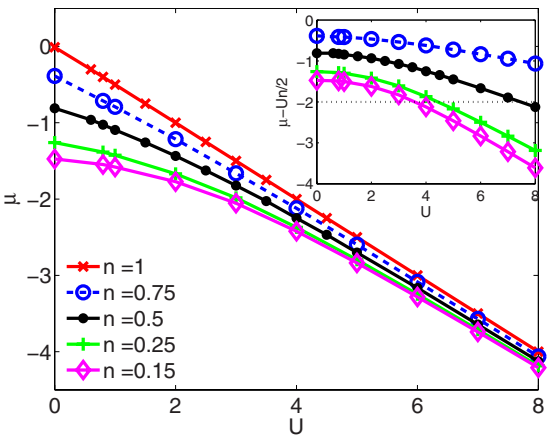

FIG. 3. (Color online) The chemical potential μ as a function of U for different filling factors n. The inset shows the quantity $\mu-Un/2$.

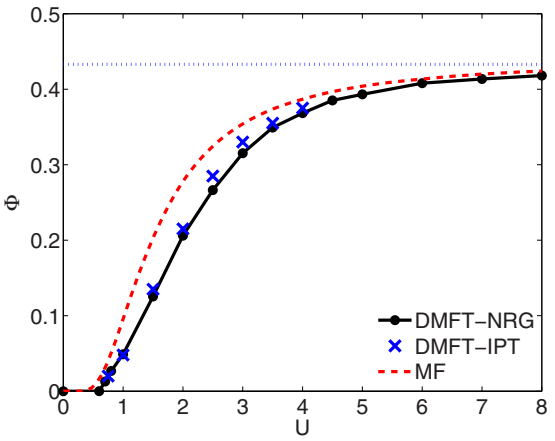

FIG. 4. (Color online) The anomalous expectation value Φ as a function of U for $n=0.5$. For comparison, we have included the results from DMFT-IPT extracted from Ref. 27 and the dashed line gives the result for Φ_{MF}.

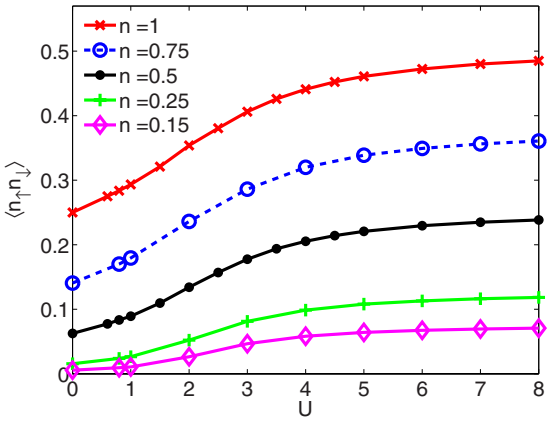

FIG. 5. (Color online) Average pair density $\langle n_\uparrow n_\downarrow \rangle$ as a function of U for a number of different filling factors.

which investigates the transition temperature as a pairing instability from the two-particle response function.[25] We expect the anomalous expectation value Φ in the strong-coupling limit to be reduced from the mean-field value due strong phase fluctuations. This is analogous to the reduction in the antiferromagnetic order parameter in the Heisenberg model by (transverse) spin waves. The latter is, however, not captured within our DMFT calculations in the state with broken symmetry, and Φ increases to a constant as in the mean-field theory, as can be seen in Fig. 4 for quarter filling.

The order parameter $\Delta_{\mathrm{sc,DMFT}}=U\Phi_{\mathrm{DMFT}}$ can, however, be interpreted as a high-energy scale for the pair formation then.[15] The DMFT results for Φ_{DMFT} are obtained by the integration of the off-diagonal Green's function as in Eq. (46) or the static expectation values calculated in the NRG procedure; the results of which are in very good agreement. MF and DMFT results show qualitatively a very similar overall behavior. There is a substantial reduction in the value through the quantum fluctuations included in the DMFT-NRG result, which appear most pronounced in the intermediate coupling regime, near unitarity $U_c=2$. However, also at weak coupling there is already a correction to the mean-field results. For instance, at $U=0.7$, we find $\Phi_{\mathrm{MF}}/\Phi_{\mathrm{DMFT}}\approx 2.58$. This is comparable to the reduction found in the analysis of Martín-Rodero and Flores[44] with the second-order perturbation theory. Below $U=0.5$, the ordering scale is very small, and we do not find a well-converged DMFT solution with symmetry breaking any more. In Fig. 4, we have also included the results obtained by the DMFT-IPT,[27] which are slightly larger but otherwise in good agreement with our DMFT-NRG results.

C. Pair density

The ground state of the system is also characterized by the double occupancy $\langle n_\uparrow n_\downarrow \rangle$ or average pair density. The double occupancy multiplied by U gives the expectation value of the potential energy. At weak-coupling, potential energy is gained in the symmetry broken state; whereas at strong-coupling, kinetic-energy gain is usually responsible for Bose-Einstein condensation. $\langle n_\uparrow n_\downarrow \rangle$ can be calculated directly from NRG expectation values. In Fig. 5, it is plotted for different filling factors for a range of interactions.

In the noninteracting limit, it is given by $(n/2)^2$ since the particles are uncorrelated and the probabilities $n/2$ to find a particle with spin σ are just multiplied. In the strong-coupling limit, all particles are bound to pairs, and the pair density is given by half the filling factor $\langle n_\uparrow n_\downarrow \rangle = n/2$. This continuous crossover from the noninteracting to the strong-coupling values can be seen for all densities with the most visible change in the intermediate coupling regime occurring around $U_c=2$.

D. Momentum distribution

On the mean-field level, the weight of the quasiparticle peaks is given directly by the factors u_k^2 and v_k^2 as seen in Eq. (49). These factors also describe the momentum distribution $n_k^{\mathrm{MF}}=v_k^2$. The corresponding DMFT result for the momentum distribution is given by the integral over the diagonal Green's function,

$$n_k = \int_{-\infty}^{0} d\omega[-\mathrm{Im}\, G_k(\omega)]/\pi. \tag{51}$$

In Fig. 6, we plot the momentum distribution n_k calculated from Eq. (51) in comparison with the mean-field result for $n=0.5$.

For small attraction ($U=1$), we can see that n_k shows the typical form known from the BCS theory dropping from one to zero in a small range around $\varepsilon_k=\mu-Un/2$. Therefore, some momentum states above $\mu-Un/2$ are occupied but only in a small region of the size of the order parameter. When U is increased, the momentum distribution is spread over a larger range. In the BEC limit, where the fermions are tightly bound and therefore very localized in position space, we expect the momentum distribution to be spread due to the uncertainty principle. In all cases, the sum rule $1/N\Sigma_k n_k = n/2$ is satisfied numerically within an accuracy of about 1%. There are visible quantitative deviations between MF and DMFT results, but they are fairly small. Our results are

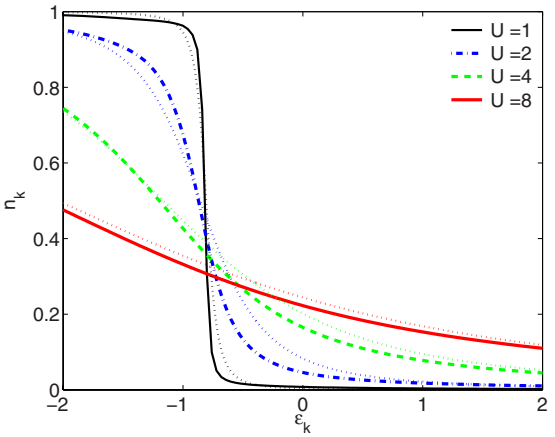

FIG. 6. (Color online) The momentum distribution calculated from the $\boldsymbol{k}$-dependent Green's function and compared with the MF result $n_{\boldsymbol{k}}^{\mathrm{MF}}=v_{\boldsymbol{k}}^2$ (dotted lines) for $n=0.5$.

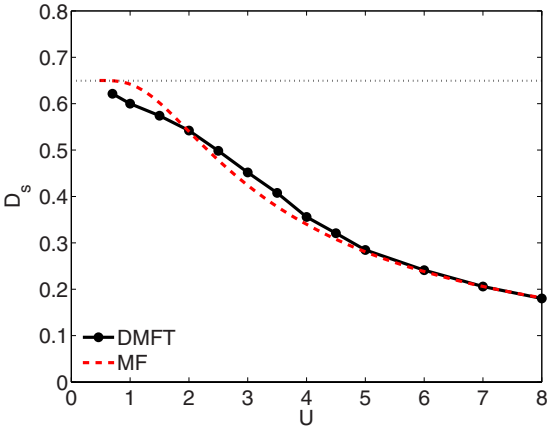

FIG. 7. (Color online) The superfluid stiffness D_s as calculated from the off-diagonal Green's function in Eq. (56) for $n=0.5$. The dashed line gives the result for D_s, when evaluated as in Eq. (57).

well comparable to the ones presented by Garg *et al.*[27]

In the experiments in ultracold gases where the BCS-BEC crossover is investigated, the momentum distribution can be measured quite accurately. This has been studied also in comparison with mean-field results by Regal *et al.*[45] Considering low densities for the lattice system and taking into account that an additional broadening would occur at finite temperature, a qualitative agreement of our results with the experiment can be found.

E. Superfluid stiffness

For a system in a coherent superfluid state, another characteristic quantity is the superfluid stiffness D_s. It is a measure of the energy required to twist the phase of the condensate and therefore related to the degree of phase coherence of the superconducting state. Usually, it is proportional to the superfluid density n_s, which is experimentally accessible via the penetration length. Toschi *et al.*[16] investigated the relation between T_c and D_s in the attractive Hubbard model and found that a linear scaling relation, as in the Uemura plot, holds at intermediate and strong coupling.

D_s can be calculated either from the weight of the delta-function in the optical conductivity or from the transverse part of the current-current correlation function[16] $\chi_{j_\perp;j_\perp}(\boldsymbol{q},\omega)$,

$$D_s = D_{\mathrm{dia}} - \chi_{j_\perp;j_\perp}(\boldsymbol{q}\to 0,\omega=0). \tag{52}$$

The diamagnetic term D_{dia} is essentially given by the kinetic energy,

$$D_{\mathrm{dia}} = -\frac{2}{\beta}\sum_n \int d\varepsilon_{\boldsymbol{k}}\rho_0(\varepsilon_{\boldsymbol{k}})\varepsilon_{\boldsymbol{k}}G_{\boldsymbol{k}}(i\omega_n), \tag{53}$$

where $G_{\boldsymbol{k}}(i\omega_n)$ is the Matsubara Green's function. In the infinite-dimensional limit, $\chi_{j_\perp;j_\perp}$ reduces to the bubble of normal and anomalous propagators.[16,46] From this and the relation $-\partial/\partial\varepsilon_{\boldsymbol{k}}[\rho_0(\varepsilon_{\boldsymbol{k}})V(\varepsilon_{\boldsymbol{k}})]=\rho_0(\varepsilon_{\boldsymbol{k}})\varepsilon_{\boldsymbol{k}}$ and integration by parts, one finds that the diamagnetic term cancels, which yields[16]

$$D_s = \frac{4}{\beta}\sum_n \int d\varepsilon_{\boldsymbol{k}}\rho_0(\varepsilon_{\boldsymbol{k}})V(\varepsilon_{\boldsymbol{k}})G_{\boldsymbol{k}}^{\mathrm{off}}(i\omega_n)G_{\boldsymbol{k}}^{\mathrm{off}}(i\omega_n), \tag{54}$$

where $V(\varepsilon_{\boldsymbol{k}})=(4t^2-\varepsilon_{\boldsymbol{k}}^2)/3$ for the Bethe lattice. We can use the spectral representation,

$$G_{\boldsymbol{k}}^{\mathrm{off}}(i\omega_n) = \int d\omega' \frac{\rho_{\boldsymbol{k}}^{\mathrm{off}}(\omega')}{i\omega_n-\omega'} \tag{55}$$

and the Kramers-Kronig relations for the real and imaginary parts of the Green's function such that at zero temperature D_s takes the form,

$$D_s = -\frac{8}{\pi}\int d\varepsilon_{\boldsymbol{k}}\rho_0(\varepsilon_{\boldsymbol{k}})V(\varepsilon_{\boldsymbol{k}})\int_{-\infty}^{0} d\omega\ \mathrm{Im}\ G_{\boldsymbol{k}}^{r,\mathrm{off}}(\omega)\mathrm{Re}\ G_{\boldsymbol{k}}^{r,\mathrm{off}}(\omega), \tag{56}$$

where $G_{\boldsymbol{k}}^{r,\mathrm{off}}(\omega)$ is the retarded off-diagonal Green's function (5). We can evaluate the expression (56) using the mean-field Green's function in the form (50), which yields the somewhat simpler expression

$$D_s^{\mathrm{MF}} = 4\int_{-D}^{D} d\varepsilon_{\boldsymbol{k}}\rho_0(\varepsilon_{\boldsymbol{k}})V(\varepsilon_{\boldsymbol{k}})\frac{u_{\boldsymbol{k}}^2v_{\boldsymbol{k}}^2}{E_{\boldsymbol{k}}^0}. \tag{57}$$

This expression can be evaluated in the limit $U\to 0$, $\Delta_{\mathrm{sc}}\to 0$ as $u_{\boldsymbol{k}}^2v_{\boldsymbol{k}}^2/E_{\boldsymbol{k}}^0$ goes to a delta function then, and hence $D_s\to 2\rho_0(\bar{\mu})V(\bar{\mu})$.

In Fig. 7, the superfluid stiffness D_s calculated from Eq. (56) is displayed as a function of U for quarter filling. The dashed line shows the result as obtained from Eq. (57), where the mean-field Green's functions are used to evaluate the integrals.

We can see that the results for D_s of DMFT and MF calculation do not deviate very much. The superfluid stiffness is maximal in the BCS limit and decreases to smaller values in the BEC limit. D_s is proportional to the inverse of the effective mass of the pairs $m_B\sim U/t^2$ and therefore expected to decrease like $1/U$. The system in this limit consists

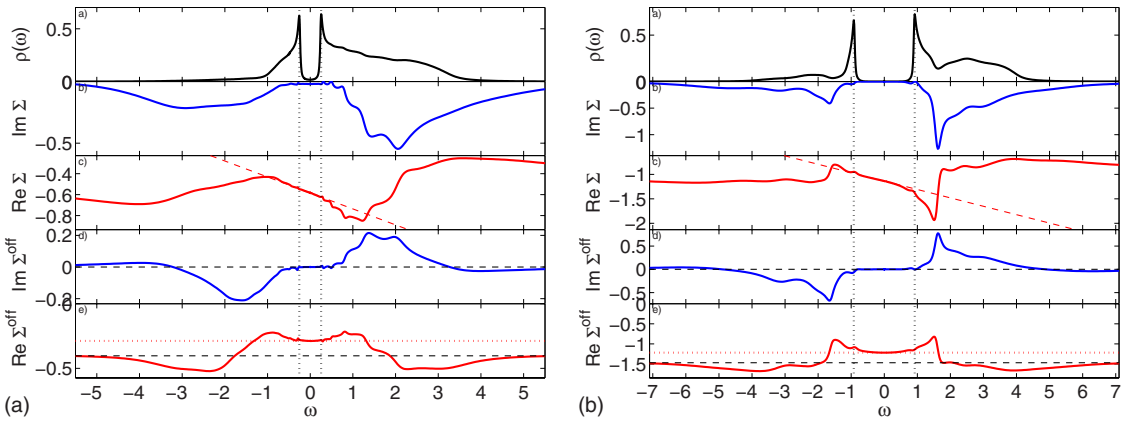

FIG. 8. (Color online) The spectral functions, imaginary, and real parts of the diagonal and off-diagonal self-energies plotted for $U=2$ (left) and $U=4$ (right) with $b=0.2$ and $n=0.5$. The dotted vertical line gives the peak position of the spectral function, which can be roughly identified with E_g.

of heavy weakly interacting bosons, with less phase coherence. The results shown are in agreement with the ones reported by Toschi *et al.*[16]

Summarizing this section, we see that our DMFT-NRG results for chemical-potential, static, and integrated properties at zero temperature are in good agreement with earlier calculations based on different impurity solvers. In fact most of the results are in good agreement with mean-field theory and quantitative deviations due to the fluctuations included in DMFT are not very large. One could therefore argue that the main features are already fairly well described by the simpler static mean-field treatment. In the next section, we will turn to spectral quantities. In contrast, there certain features such as the distinction of coherent and incoherent excitations can only be described when we go beyond the mean-field theory. Some of these extra features found in the spectral resolution are lost again when considering integrated quantities.

VI. SPECTRAL FUNCTIONS

In this section, we present our DMFT-NRG results for the local spectral density $\rho(\omega)$ and the $\boldsymbol{k}$-resolved spectra, $\rho_{\boldsymbol{k}}(\omega)=-\mathrm{Im}\, G_{\boldsymbol{k}}(\omega)/\pi$, in the different parameter regimes. Before discussing these results in detail and comparing them with those of Garg *et al.*,[27] we consider the different types of approximations used in the IPT and NRG calculations. These are relevant in assessing the two sets of results to arrive at a clearer physical interpretation.

The approximation used in the IPT is in restricting the calculation to the second-order diagram for the self-energy. This is evaluated using the Hartree-Bogoliubov-corrected propagator for the effective impurity. If this propagator has a spectral density with a gap E_g then the imaginary part of the self-energy from this second-order scattering term can only develop in the regime $|\omega|>3E_g$. This threshold energy of $3E_g$ corresponds to the minimum energy for a fermion above the gap E_g to emit a quasiparticle-quasihole pair excitation. Therefore, in the IPT, the single-particle spectral functions $\rho_{\boldsymbol{k}}(\omega)$ have isolated delta-function peaks corresponding to the Bogoliubov quasiparticle excitations with minimal energy E_g, together with incoherent continuous spectrum for $|\omega|>3E_g$.

In applying the NRG approach to the effective impurity problem, approximations arise in using a discrete spectrum for the conduction-electron bath. The spectral functions are calculated as Lehmann sums over delta-function peaks, the positions of the peaks being deduced from the discrete many-body energy levels, and their weighting from the corresponding matrix elements. This is also the case for other methods using numerical diagonalization such as the ED method. To obtain a continuous spectral function, these delta-function peaks have to be broadened appropriately, usually with a lognormal function with parameter b.[20] If the broadening is too large certain features blur, if it is too small the spectral functions has many spikes and is difficult to interpret. With such a broadening procedure, it is difficult to resolve sharp features such as a gap in the spectrum and hence an energy E_g. However, usually an estimate of the gap can be made when the broadening is taken into account. For all the previous results on static and integrated quantities, we have used a conventional broadening parameter $b=0.5$, and the results for these quantities depend very little on the broadening. In MF theory, Φ increases exponentially at weak coupling. At strong coupling it only depends on the density n as seen in Eq. (48).

Another aspect of the NRG calculations that can lead to some numerical uncertainty is in the way the self-energy is calculated. In Eq. (A15), it is shown how the self-energy can be calculated from the matrices of the Green's function $\underline{G}$ and the higher Green's function $\underline{F}$. If one is interested in the values of ω for which the imaginary part of the self-energy vanishes then the whole expression in Eq. (A15) has to be considered. As is well known for NRG calculations for the Anderson impurity model,[20] the condition $\mathrm{Im}\,\Sigma(0)=0$ for the Friedel sum rule can be reasonably well satisfied. However, $\mathrm{Im}\,\Sigma$ is never exactly zero and numerical errors can often be seen in small imaginary parts of the self-energy from this procedure.

In Fig. 8, we present the NRG results for the local spectral density $\rho(\omega)$ and the real and imaginary parts for the diagonal and off-diagonal self-energies for $U=2$ and $U=4$. We see

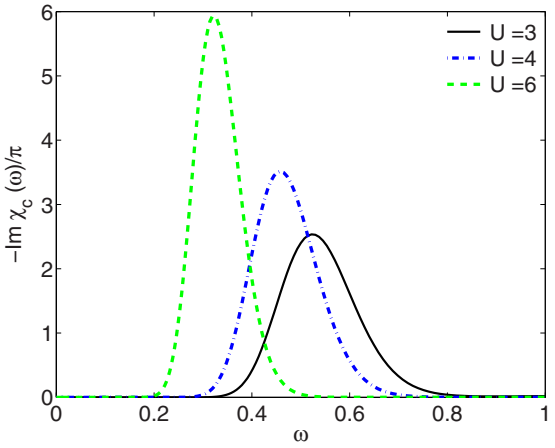

FIG. 9. (Color online) The imaginary part of the local charge susceptibility for $U=3,4,6$ ($b=00.2$). We find strong excitations corresponding to charge fluctuations there below the respective estimates of $E_g \simeq 0.5, 0.9, 1.7$.

that Im Σ and Im Σ^{off} are approximately zero for a certain range of ω for both cases. Im Σ^{off} is an antisymmetric function, which has peaks at similar positions as Im Σ. Re Σ^{off} is a symmetric function which for large ω tends to the value $\Delta_{\text{sc}}=U\Phi$ of the interacting system (46) and for small ω can be interpreted as a renormalized gap.

In the weaker coupling case $U=2$, we find a trend similar to the IPT in that Im Σ deviates appreciably from zero only when $|\omega|>3E_g$. This can be seen on closer inspection of the top part of Fig. 8, where we estimate $E_g \approx 0.25$, and Im $\Sigma > 0$ for roughly $\omega > 0.75$ (the wiggles for smaller ω are interpreted as inaccuracies). This means that in the corresponding spectrum for $\rho_k(\omega)$, there are isolated quasiparticle peaks and a continuous incoherent part in the spectrum for $|\omega| > 3E_g$. The widths of the quasiparticles peaks, however, will not be precisely zero as in the IPT due to the very small imaginary parts. In the spectrum for $\rho(\omega)$ and $U=2$ shown in Fig. 8, there is a sharp peak due to the quasiparticle excitations in $\rho(\omega)$ just above the gap (see also Fig. 1 in Ref. 24). This quasiparticle band is very similar to the one based on the IPT presented in Fig. 3 in Ref. 27. In the IPT case, there is a square-root singularity at the gap edge which does not appear in the NRG results due to the small imaginary part in the self-energies.

This picture changes in the stronger coupling case $U=4$. Here it can be seen that the imaginary parts of both the diagonal and off-diagonal self-energies develop a pronounced peak which falls within the region $E_g<|\omega|<3E_g$. This leads to incoherent spectral weight in $\rho_k(\omega)$ for $|\omega| < 3E_g$. This is a difference with the IPT results where the imaginary parts of the self-energy are always zero for $E_g < |\omega| < 3E_g$ and, consequently, there is no incoherent part of the spectrum for $\rho_k(\omega)$ in the range $|\omega|<3E_g$. An explanation for this difference can be found by examining what happens to the local dynamical charge susceptibility $\chi_c(\omega)$ as U increases. Results for $\chi_c(\omega)$ for $U=3,4,6$ are shown Fig. 9. The excitation gap Δ_c in this spectrum can be seen to decrease significantly as U increases. In Ref. 24 it was found[47] that at strong coupling, Δ_c decreases like $\sim t^2/U$. In the weak-coupling case $\Delta_c \sim 2E_g$, but for strong coupling E_g increases with U, while Δ_c decreases. Therefore, the contribution to the self-energy arising from the scattering with charge fluctuations can—for larger U—generate a finite imaginary part of the self-energy for $E_g<|\omega|<3E_g$. The location of the peak in Im Σ appears consistent with such an interpretation. The same effect cannot arise from scattering with the spin fluctuations, as these have a larger characteristic energy scale (on the order of U). For a further discussion of the behavior of the charge and spin gap, we refer to Ref. 24.

The development of the peak in the imaginary part of the self-energy in the range $|\omega|<3E_g$ leads to a dip in the local spectral function $\rho(\omega)$ for $U=4$ as can be seen in Fig. 8. There is then a peak-dip-hump structure in $\rho(\omega)$ for $U=4$ (see also Fig. 11). This feature has also been found in calculations for the attractive continuum model.[48] This behavior is not visible in the IPT calculations (cf. Fig. 3 in Ref. 27). The most likely explanation is the restriction in the IPT to the second-order diagram, which does not allow for any renormalization of the charge fluctuations.

We now consider the effect of increasing U in the quasiparticle excitations which can be seen in the results for the spectral function $\rho_k(\omega)$ for $U=1$ and $U=4$ for quarter filling shown in Fig. 10. For both cases $U=1$ and $U=4$, we can see a series of sharp quasiparticle peaks which are most narrow in the region $\varepsilon_k \approx \bar{\mu}$, which is also the point where the spectral gap is minimal. In the latter case $U=4$ in addition, we find the hump with incoherent spectral weight as discussed earlier for $\rho(\omega)$. We have also added arrows which indicate the position of the quasiparticle peaks $\pm E_k^0$ in mean-field theory (49), and the height gives the spectral weight. We can see that they describe the position of the quasiparticle excitation well for $U=1$. For the larger U case, the structure in the spectral function is not so well captured by the single quasiparticle peaks of the mean-field theory. The energy of the quasiparticle excitations differs markedly from the mean-field prediction and there is a significant transfer of spectral weight to the incoherent hump, in particular, at high energy. The quasiparticle band (weight and bandwidth) at low energy is, however, captured on a qualitative level by the mean-field theory. The quasiparticle peaks for $\rho_k(\omega)$ always have a finite width since our self-energy is never strictly zero. One can infer the bands from the poles of the Green's function E_k and compare them with the mean-field bands $\pm E_k^0$. For the weak coupling, they are in good agreement. Toward the BEC limit, the effective mass m_B of a boson pair is on the order U. This is reflected in the smaller effective bandwidth for the case $U=4$ (Fig. 10). The weight of the peaks in the full spectrum $\rho_k(\omega)$ is in accordance with the height of the arrows for $\rho_k^0(\omega)$. We can see that in the BCS limit (left), the weight in the lower band decreases rapidly to zero near $\varepsilon_k=\bar{\mu}$; whereas toward the BEC limit (right) it spreads over a much larger region which corresponds to what has been observed for momentum distributions in Fig. 6.

In earlier work,[24] the quasiparticle properties were analyzed in an expansion around the solutions E_k of the equation Re $G_k(\omega=E_k)^{-1}=0$. This led to the Lorentz-like quasiparticle peak of the form

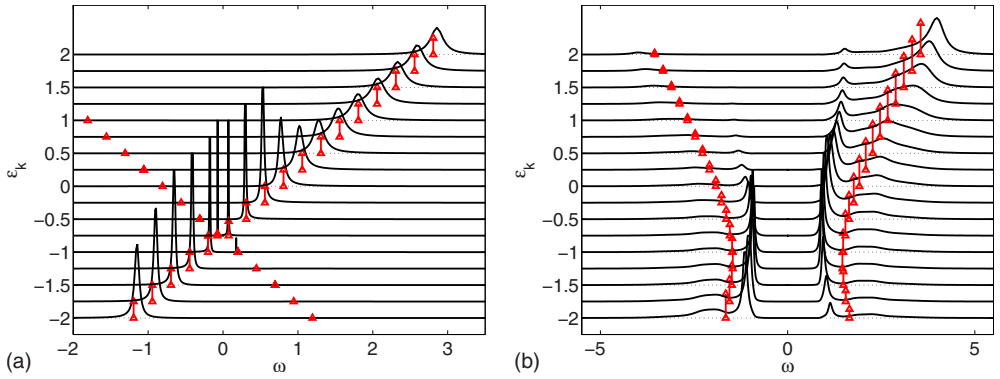

FIG. 10. (Color online) The ε_k-resolved spectral functions $\rho_k(\omega)$ for quarter filling in the BCS limit $U=1$ (left) and toward the BEC limit $U=4$ ($b=0.2$) (right). The arrows show the delta-function peaks of the mean-field solution $\rho_k^0(\omega)$, where the height of the arrow indicates the weight of the peak.

$$\rho_k(\omega) = w_+(E_k)\frac{W(E_k)/\pi}{(\omega - E_k)^2 + W(E_k)^2}, \tag{58}$$

with width $W(E_k)$ and weight $w_+(E_k)$. When a standard broadening of $b=0.5$ is used, one finds a finite width of the peaks which increases in the crossover regime leading to a strongly reduced lifetime of the quasiparticles. In the more careful analysis here with smaller broadening and taking into account possible errors in determining the self-energy, we come to the conclusion that this is not generally correct. We should not expect a finite imaginary part of the self-energy to appear for $\omega \simeq E_g$ in a DMFT calculation which does not include collective modes.[49]

Being aware of limitations in our numerical calculations, we investigate in more detail how the one-particle spectra near the minimal spectral gap modify from weak to intermediate coupling. Here we use a general scheme in which we analyze the peaks in the spectral function directly numerically and estimate the transfer of weight from the quasiparticle peaks to the incoherent part of the spectrum. We take the peak position in $\rho_k(\omega)$ for a given ε_k as the excitation energy E_k^{ex}, the full width F_{peak} at half maximum as the width, and the weight is determined by the integration over a region around E_k^{ex} of $2F_{\mathrm{peak}}$. Such an analysis also applies to antisymmetric peak forms and is equivalent to the other one for sharp Lorentz-like peaks. Note that a normalized Lorentz peak with width Δ (half width at half maximum) integrated from -2Δ to 2Δ yields the spectral weight $w_{2\Delta} = 2\arctan(2)/\pi \approx 0.705$.

We have done such an analysis for the ε_k-resolved spectral functions, where we consider an ε_k such that the excitation gap is minimal. The corresponding spectral functions for $U=1-4$ are displayed in Fig. 11. We have included a line at half maximum for the width as well as marked the integration area in the low-energy peak. We can see now very clearly how the spectrum changes from one coherent quasiparticle peak at weak coupling to the peak-dip-hump structure at intermediate coupling. This is similar to what was found in the calculation for an attractive continuum model,[48] where a sharp quasiparticle peak with little weight is still present at strong coupling. In our calculation, the strong-coupling limit is not easy to analyze as we always have some finite imaginary part of the self-energy leading to a finite width of the quasiparticle peak, which is partly spurious and tends to be larger at large coupling. At strong coupling, the excitations occur at higher energy and we have to reduce the broadening further, which leads to a more spiky spectrum. It should be mentioned that if the broadening is chosen larger (e.g., $b=0.5$) then there is only one broad peak in the spectral function.

The estimate of the weight of the quasiparticle peak w_{peak} extracted by the integration is plotted in Fig. 12 as a function of U. For weak coupling $U \simeq 1$, we would expect the mean-field result $v_k^2(\varepsilon_k = \bar{\mu}) = 0.5$. Due to the reduced integration range, we find $w_{\mathrm{peak}} \approx 0.34$; but division by $w_{2\Delta}$ gives a value close to 0.5.

Coming from weak coupling, we find a decrease as spectral weight is transferred to incoherent parts as seen before in Fig. 11. This resembles the results of Ref. 48.

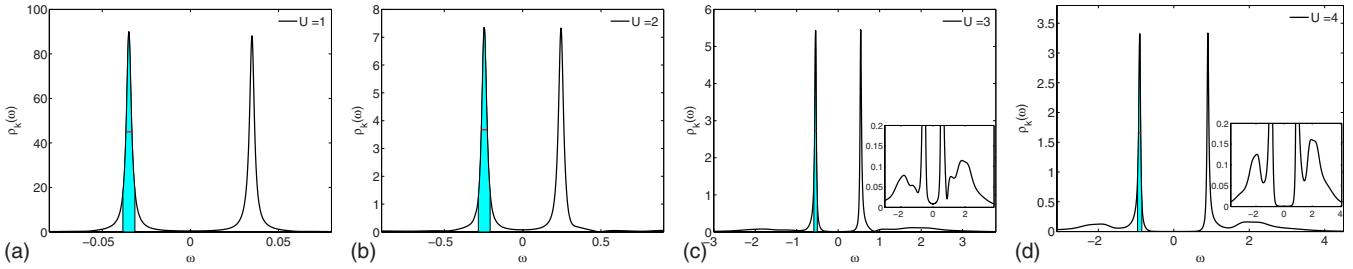

FIG. 11. (Color online) The spectral functions $\rho_k(\omega)$ for an ε_k where the gap is minimal for quarter filling and $U=1-4$ ($b=0.2$). The integration area, which gives the weight of the peaks, is shown.

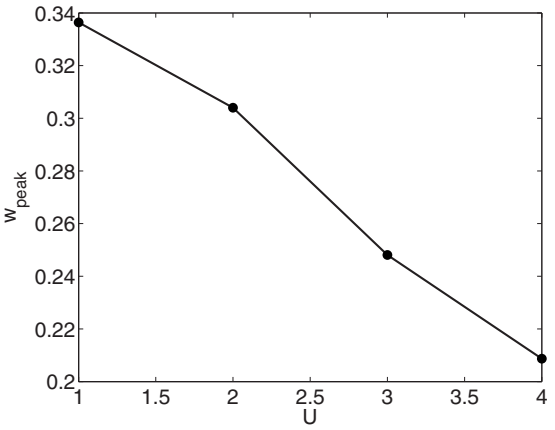

FIG. 12. The weight of the peak for spectral excitation as a function of U for quarter filling.

As discussed before due to the uncertainty about the imaginary part of the self-energy at low frequency, the behavior of the width F_{peak} cannot be reliably estimated. At weak coupling, we expect the prediction of a real delta-function with $F_{\text{peak}} \to 0$ to hold. Whether at strong-coupling low enough excitations can be generated to change this remains to be answered. We stress here again that the conclusions about the behavior of $W(\min E_{\boldsymbol{k}})$ as given in Eq. (58), which was reported in Fig. 3 of Ref. 24, are found to be incorrect as judged by the present more careful interpretation of our DMFT-NRG calculations.

VII. CONCLUSIONS

In this paper, we have presented an analysis of the ground-state properties of the attractive Hubbard model in the symmetry broken phase in the BCS-BEC crossover. The emphasis has been on the evolution of spectral functions in the crossover regime. Our analysis is based on an extension of the DMFT-NRG method to the case with superconducting symmetry breaking. We have given many details of this extension in Sec. III and in Appendices A and B. At half filling, we have related our approach both for the effective impurity model and for the lattice quantities to earlier DMFT-NRG calculations with antiferromagnetic symmetry breaking. A good agreement has been found there, which validates the applicability of our approach. As emphasized in Ref. 24, apart from the attractive Hubbard model the extended method can be useful to study superconductivity in other models, such as the Hubbard-Holstein type, and also questions related to the microscopic description of magnetic impurities in superconductors, which require self-consistent treatments.

We have discussed our DMFT-NRG results for static and integrated quantities such as the anomalous expectation value, the double occupancy, or superfluid stiffness. The results for these are in good agreement with earlier calculations based on different impurity solvers, and it has been found that most of the results are already obtained qualitatively well on the mean-field level.

The main interest of this paper has been to study the fermionic spectrum throughout the crossover regime. The local dynamics are very well described in our DMFT-NRG approach. We discussed how the behavior of the dynamic self-energies changes when the interaction becomes larger. At weak coupling, the spectrum is dominated by sharp symmetric Bogoliubov quasiparticle peaks as known from the mean-field theory. Contributions from particle-particle and particle-hole fluctuations incorporated in the dynamic self-energies appear at higher energy and are small, similar to those seen in the IPT approach. However, when the local interaction is in the unitary regime and larger, the imaginary part of the dynamic self-energy shows a characteristic feature which generates a peak-dip-hump structure in the spectral function. We argued that this feature is likely to be generated by charge fluctuations as seen in the local dynamic charge susceptibility. One finds that the spectral weight is transferred into the incoherent parts (hump) of the spectrum in increasing the coupling.

To answer the question whether at strong coupling the fermionic quasiparticles acquire a finite width, one needs to clarify over which region the imaginary parts of the self-energies vanish. Unfortunately, our method, in which spectral functions are obtained after broadening delta-peaks, is not accurate enough at present to allow for definite statements. It is possible that the peaks always remain sharp in the limit of infinite dimensions. Our DMFT approach does not capture spatial fluctuations and the gapless Goldstone mode. It would also be of great interest to study how such effects give a modification of the discussed fermionic spectrum[50,51] and possibly a suppression of the quasiparticle peaks.

ACKNOWLEDGMENTS

We wish to thank W. Metzner, A. Oguri, P. Strack, and A. Toschi for helpful discussions, W. Koller and D. Meyer for their earlier contributions to the development of the NRG programs, and R. Zeyher for critically reading the paper.

APPENDIX A: NRG FORMALISM WITH SUPERCONDUCTING SYMMETRY BREAKING

1. Mapping to the linear chain

The second important step (ii) in the self-consistent NRG procedure is to map the discretized model (13) to the so-called linear-chain model of the general form (28),

$$H_{\text{And}} = \sum_{\sigma,n=0}^{N} \varepsilon_n f_{n,\sigma}^{\dagger} f_{n,\sigma} + \sum_{\sigma,n=-1}^{N} \beta_n (f_{n,\sigma}^{\dagger} f_{n+1,\sigma} + \text{H.c.}) - \sum_{n=0}^{N} \Delta_n (f_{n,\uparrow}^{\dagger} f_{n,\downarrow}^{\dagger} + f_{n,\downarrow} f_{n,\uparrow}). \tag{A1}$$

The orthogonal transformation has been chosen in the form [cf. Eq. (31)],

$$f_{n,\uparrow} = \sum_{\alpha,m} u_{\alpha,nm} a_{\alpha,m,\uparrow} - v_{\alpha,nm} a_{\alpha,m,\downarrow}^{\dagger}, \tag{A2}$$

$$a_{\alpha,m,\uparrow} = \sum_{n} u_{\alpha,nm} f_{n,\uparrow} + v_{\alpha,nm} f_{n,\downarrow}^{\dagger}, \tag{A3}$$

$$f^{\dagger}_{n,\downarrow} = \sum_{\alpha,m} v_{\alpha,nm} a_{\alpha,m,\uparrow} + u_{\alpha,nm} a^{\dagger}_{\alpha,m,\downarrow}, \tag{A4}$$

$$a^{\dagger}_{\alpha,m,\downarrow} = \sum_{n} -v_{\alpha,nm} f_{n,\uparrow} + u_{\alpha,nm} f^{\dagger}_{n,\downarrow}. \tag{A5}$$

The matrix elements of the transformation obey the relations

$$\sum_{n} u_{\alpha,nm} u_{\alpha',nm'} + v_{\alpha,nm} v_{\alpha',nm'} = \delta_{m,m'} \delta_{\alpha,\alpha'},$$

$$\sum_{m,\alpha} u_{\alpha,nm} u_{\alpha,n'm} + v_{\alpha,nm} v_{\alpha,n'm} = \delta_{n,n'},$$

and

$$\sum_{m,\alpha} u_{\alpha,nm} v_{\alpha,n'm} - v_{\alpha,nm} u_{\alpha,n'm} = 0,$$

$$\sum_{n} u_{\alpha,nm} v_{\alpha',nm'} - v_{\alpha,nm} u_{\alpha',nm'} = 0,$$

which ensure that both operator sets satisfy canonical anticommutation relations. We can now derive the recursion relations for the matrix elements and the parameters. This is done in analogy to earlier work by Bulla *et al.*[39] We equate the representations for the media of Eqs. (13) and (A1) and substitute the operator transformations (A2)–(A5). One can then read off the coefficients of the $f_{n,\uparrow}$ operators ($n>0$) on both sides of the equation, which yields

$$\begin{aligned}
&\sum_{n',\alpha} \xi^{\alpha}_{n'} (u_{\alpha,nn'} a^{\dagger}_{\alpha,n',\uparrow} + v_{\alpha,nn'} a_{\alpha,n',\downarrow}) \\
&\quad + \sum_{n',\alpha} \delta^{\alpha}_{n'} (v_{\alpha,nn'} a^{\dagger}_{\alpha,n',\uparrow} - u_{\alpha,nn'} a_{\alpha,n',\downarrow}) \\
&\quad = \varepsilon_n f^{\dagger}_{n,\uparrow} + \beta_{n-1} f^{\dagger}_{n-1,\uparrow} + \beta_n f^{\dagger}_{n+1,\uparrow} - \Delta_n f_{n,\downarrow}.
\end{aligned}$$

From this we find the expression (33) for ε_n by taking the anticommutator with $f_{n,\uparrow}$. The anticommutator with $f^{\dagger}_{n,\downarrow}$ gives the expression (34) for Δ_n. With the representations (A2)–(A5), we can modify Eq. (A6) to obtain

$$\begin{aligned}
\beta_n f^{\dagger}_{n+1,\uparrow} = &\sum_{n',\alpha} [(\xi^{\alpha}_{n'} - \varepsilon_n) u_{\alpha,nn'} + (\delta^{\alpha}_{n'} + \Delta_n) v_{\alpha,nn'} \\
&- \beta_{n-1} u_{\alpha,n-1n'}] a^{\dagger}_{\alpha,n',\uparrow} + \sum_{n',\alpha} [(\Delta_n - \delta^{\alpha}_{n'}) u_{\alpha,nn'} \\
&+ (\xi^{\alpha}_{n'} + \varepsilon_n) v_{\alpha,nn'} + \beta_{n-1} v_{\alpha,n-1n'}] a_{\alpha,n',\downarrow}.
\end{aligned}$$

By comparison with Eq. (31), we can read off a recursion relation for $u_{\alpha,n+1n'}$ in Eq. (36) and for $v_{\alpha,n+1n'}$ as in Eq. (37). The recursion relation for β_n is obtained from the anticommutator of with $f_{n+1,\uparrow}$ which yields

$$\beta^2_n = \sum_{n',\alpha} (u^2_{\alpha,n+1n'} + v^2_{\alpha,n+1n'}).$$

With the orthonormality relations and the definitions ε_n and Δ_n, we can find the expression in Eq. (35).

2. Relevant Green's functions

In this section. we briefly outline some details for the calculations of the relevant Green's functions and the self-energy for completeness.[37] For the Green's functions, it is convenient to work in Nambu space, $\boldsymbol{C}^{\dagger}_d = (d^{\dagger}_{\uparrow}, d_{\downarrow})$, with 2×2 matrices. The relevant retarded Green's functions are then

$$\underline{G}_d(\omega) = \langle\langle \boldsymbol{C}_d; \boldsymbol{C}^{\dagger}_d \rangle\rangle_{\omega} = \begin{pmatrix} \langle\langle d_{\uparrow}; d^{\dagger}_{\uparrow} \rangle\rangle_{\omega} & \langle\langle d_{\uparrow}; d_{\downarrow} \rangle\rangle_{\omega} \\ \langle\langle d^{\dagger}_{\downarrow}; d^{\dagger}_{\uparrow} \rangle\rangle_{\omega} & \langle\langle d^{\dagger}_{\downarrow}; d_{\downarrow} \rangle\rangle_{\omega} \end{pmatrix}. \tag{A6}$$

In the NRG approach, we calculate G_{11} and G_{21} directly and infer $G_{22}(\omega) = -G_{11}(-\omega)^*$, which follows from $G^{\mathrm{ret}}_{A,B}(\omega) = -G^{\mathrm{adv}}_{B,A}(-\omega)$ and $G^{\mathrm{ret/adv}}_{A,B}(\omega) = -G^{\mathrm{ret/adv}}_{A^{\dagger},B^{\dagger}}(-\omega)^*$ for fermionic operators A, B. Similarly, we can find $G_{12}(\omega) = G_{21}(-\omega)^*$. In the derivation, one has to be careful and include a sign change for up down-spin interchange in the corresponding operator combination.

In the noninteracting case, we can deduce the d-site Green's function matrix of the model Hamiltonian (6) exactly. To do so, we rewrite the superconducting term of the medium H_{sc} by introducing the vector of operators and the symmetric matrix

$$\boldsymbol{C}_{\boldsymbol{k}} := \begin{pmatrix} c_{\boldsymbol{k},\uparrow} \\ c^{\dagger}_{-\boldsymbol{k},\downarrow} \end{pmatrix}, \quad A_{\boldsymbol{k}} := \begin{pmatrix} \varepsilon_{\boldsymbol{k}} & -\Delta_{\boldsymbol{k}} \\ -\Delta_{\boldsymbol{k}} & -\varepsilon_{\boldsymbol{k}} \end{pmatrix}. \tag{A7}$$

Then H_{sc} can be written as

$$H_{\mathrm{sc}} = \sum_{\boldsymbol{k}} \boldsymbol{C}^{\dagger}_{\boldsymbol{k}} A_{\boldsymbol{k}} \boldsymbol{C}_{\boldsymbol{k}}. \tag{A8}$$

The matrix Green's function in the superconducting bath is then given by $\underline{g}_{\boldsymbol{k}}(i\omega_n) = (i\omega_n \mathbb{1}_2 - A_{\boldsymbol{k}})^{-1}$,

$$\underline{g}_{\boldsymbol{k}}(i\omega_n)^{-1} = i\omega_n \mathbb{1}_2 - \varepsilon_{\boldsymbol{k}} \tau_3 + \Delta_{\boldsymbol{k}} \tau_1, \tag{A9}$$

where τ_i are Pauli matrices. It follows that

$$\underline{g}_{\boldsymbol{k}}(i\omega_n) = \frac{i\omega_n \mathbb{1}_2 + \varepsilon_{\boldsymbol{k}} \tau_3 - \Delta_{\mathrm{sc}} \tau_1}{(i\omega_n)^2 - (\varepsilon^2_{\boldsymbol{k}} + \Delta^2_{\boldsymbol{k}})}. \tag{A10}$$

In the noninteracting case for $T=0$, we have therefore

$$\underline{G}^0_d(\omega)^{-1} = \omega \mathbb{1}_2 - \varepsilon_d \tau_3 - \sum_{\boldsymbol{k}} V^2_{\boldsymbol{k}} \tau_3 \underline{g}_{\boldsymbol{k}}(i\omega_n) \tau_3. \tag{A11}$$

The local full Green's function matrix $\underline{G}_d(\omega)^{-1}$ for the effective impurity model is given by the Dyson matrix equation

$$\underline{G}_d(\omega)^{-1} = \underline{G}^{-1}_0(\omega) - \underline{\Sigma}(\omega), \tag{A12}$$

where $\underline{\Sigma}(\omega)$ is the self-energy matrix.

3. Self-energy using the higher F-Green's function

As described by Bulla *et al.*,[52] there is a method to calculate the self-energy employing a higher F-Green's function, and it can also be used for the case with the superconducting bath. The calculation taking into account all off-diagonal terms yields the following matrix equation:

$$\underline{G}_d^0(\omega)^{-1}\underline{G}_d(\omega) - U\underline{F}(\omega) = \mathbb{1}_2, \tag{A13}$$

with the matrix of higher Green's functions $\underline{F}(\omega)$,

$$\underline{F}(\omega) = \begin{pmatrix} F_{11}(\omega) & F_{12}(\omega) \\ F_{21}(\omega) & F_{22}(\omega) \end{pmatrix}. \tag{A14}$$

We have introduced the matrix elements $F_{11}(\omega) = \langle\langle d_\uparrow n_\downarrow; d_\uparrow^\dagger\rangle\rangle_\omega$, $F_{12}(\omega) = \langle\langle d_\uparrow n_\downarrow; d_\downarrow\rangle\rangle_\omega$, $F_{21}(\omega) = -\langle\langle d_\downarrow^\dagger n_\uparrow; d_\uparrow^\dagger\rangle\rangle_\omega$, and $F_{22}(\omega) = -\langle\langle d_\downarrow^\dagger n_\uparrow; d_\downarrow\rangle\rangle_\omega$. In the NRG, we calculate F_{11} and F_{21} and the others follow from $F_{12}(\omega) = -F_{21}(-\omega)^*$ and $F_{22}(\omega) = F_{11}(-\omega)^*$. We can define the self-energy matrix by

$$\underline{\Sigma}(\omega) = U\underline{F}(\omega)\underline{G}_d(\omega)^{-1}. \tag{A15}$$

The properties of the Green's function and the higher F-Green's function lead to the relations $\Sigma_{12}(\omega) = \Sigma_{21}(-\omega)^*$ and $\Sigma_{22}(\omega) = -\Sigma_{11}(-\omega)^*$ for the self-energies. We can therefore calculate the diagonal self-energy $\Sigma(\omega) = \Sigma_{11}(\omega)$ and the off-diagonal self-energy $\Sigma^{\text{off}}(\omega) = \Sigma_{21}(\omega)$ and deduce the other two matrix elements from them. With the relation (A15) between $\underline{G}$, $\underline{F}$, and $\underline{\Sigma}$, the Dyson equation (A12) is recovered from Eq. (A13). Therefore, once G and F are determined from the Lehmann representation, the self-energy can be calculated from Eq. (A15) and used in Eqs. (10)–(12).

APPENDIX B: MAPPING OF AFM TO SC EFFECTIVE IMPURITY MODEL

In the DMFT calculations with antiferromagnetic ordering, the effective impurity model can be given in the following discrete form:

$$H_{\text{AFM}} = \sum_{n,\alpha,\sigma} \xi_{n,\sigma}^\alpha a_{\alpha,n,\sigma}^\dagger a_{\alpha,n,\sigma} + \sum_{n,\alpha,\sigma} \gamma_{n,\sigma}^\alpha (a_{\alpha,n,\sigma}^\dagger d_\sigma + \text{H.c.}),$$

where we have omitted the impurity term. Notice that the parameters are σ dependent. In this model, the sublattice magnetic order is taken to be in the z direction, whereas in the model with superconducting symmetry breaking (13) it corresponds to a transverse direction x or y. Therefore, we first perform a rotation in spin space

$$a_{\alpha,n,\uparrow} \to \frac{1}{\sqrt{2}}(a_{\alpha,n,\uparrow} - a_{\alpha,n,\downarrow}), a_{\alpha,n,\downarrow} \to \frac{1}{\sqrt{2}}(a_{\alpha,n,\uparrow} + a_{\alpha,n,\downarrow}) \tag{B1}$$

and also for the d operators. This yields

$$\begin{aligned} H_{\text{AFM}} = & \sum_{n,\alpha,\sigma} L_n^\alpha a_{\alpha,n,\sigma}^\dagger a_{\alpha,n,\sigma} + \sum_{n,\alpha,\sigma} V_n^\alpha (a_{\alpha,n,\sigma}^\dagger d_\sigma + \text{H.c.}) \\ & - \sum_{n,\alpha} F_n^\alpha (a_{\alpha,n,\uparrow}^\dagger a_{\alpha,n,\downarrow} + a_{\alpha,n,\downarrow}^\dagger a_{\alpha,n,\uparrow}) \\ & - \sum_{n,\alpha} W_n^\alpha (a_{\alpha,n,\uparrow}^\dagger d_\downarrow + a_{\alpha,n,\downarrow}^\dagger d_\uparrow + \text{H.c.}), \end{aligned}$$

with

$$L_n^\alpha = \frac{\xi_{n,\uparrow}^\alpha + \xi_{n,\downarrow}^\alpha}{2}, \quad V_n^\alpha = \frac{\gamma_{n,\uparrow}^\alpha + \gamma_{n,\downarrow}^\alpha}{2},$$

$$F_n^\alpha = \frac{\xi_{n,\uparrow}^\alpha - \xi_{n,\downarrow}^\alpha}{2}, \quad W_n^\alpha = \frac{\gamma_{n,\uparrow}^\alpha - \gamma_{n,\downarrow}^\alpha}{2}. \tag{B2}$$

Then we do a particle- hole transformation for the down spin similar to Eq. (38),

$$a_{\alpha,n,\downarrow} \to a_{-\alpha,n,\downarrow}^\dagger, \quad d_\downarrow \to -d_\downarrow^\dagger. \tag{B3}$$

This gives

$$\begin{aligned} H_{\text{AFM}} = & \sum_{n,\alpha} L_n^\alpha (a_{\alpha,n,\uparrow}^\dagger a_{\alpha,n,\uparrow} + a_{-\alpha,n,\uparrow} a_{-\alpha,n,\downarrow}^\dagger) \\ & + \sum_{n,\alpha} V_n^\alpha (a_{\alpha,n,\uparrow}^\dagger d_\uparrow - a_{-\alpha,n,\downarrow} d_\downarrow^\dagger + \text{H.c.}) \\ & - \sum_{n,\alpha} F_n^\alpha (a_{\alpha,n,\uparrow}^\dagger a_{-\alpha,n,\downarrow}^\dagger + a_{-\alpha,n,\downarrow} a_{\alpha,n,\uparrow}) \\ & - \sum_{n,\alpha} W_n^\alpha (- a_{\alpha,n,\uparrow}^\dagger d_\downarrow^\dagger + a_{-\alpha,n,\downarrow} d_\uparrow + \text{H.c.}). \end{aligned}$$

So far we have made no assumption about the parameters $\xi_{n,\sigma}^\alpha$ and $\gamma_{n,\sigma}^\alpha$. In the usual scheme, one has $\xi_{n,\sigma}^{-\alpha} = -\xi_{n,\sigma}^\alpha$, such that $L_n^{-\alpha} = -L_n^\alpha$. Hence, the second term in the first line is identical to the standard form apart from an additional constant, when we use the fermionic anticommutation rules. In addition, $\xi_{n,\uparrow}^\alpha = \xi_{n,\downarrow}^\alpha$ is normally satisfied, such that $F_n^\alpha = 0$. Therefore, the term in the third line, which looks like the one for superconducting symmetry breaking, vanishes. We focus on the half filling case where one additionally has $\gamma_{n,\uparrow}^\alpha = \gamma_{n,\downarrow}^{-\alpha}$ So the other terms remain and one has a normal and an anomalous hopping term,

$$\begin{aligned} H_{\text{AFM}} = & \sum_{n,\alpha,\sigma} L_n^\alpha a_{\alpha,n,\sigma}^\dagger a_{\alpha,n,\sigma} + \sum_{n,\alpha,\sigma} V_n^\alpha (a_{\alpha,n,\sigma}^\dagger d_a + \text{H.c.}) \\ & + \sum_{n,\alpha} W_n^\alpha (a_{\alpha,n,\uparrow}^\dagger d_\downarrow^\dagger + d_\uparrow a_{\alpha,n,\downarrow} + \text{H.c.}). \end{aligned}$$

One can then do a Bogoliubov transformation,

$$\begin{pmatrix} a_{\alpha,n,\uparrow} \\ a_{\alpha,n,\downarrow}^\dagger \end{pmatrix} = \begin{pmatrix} u_{n,\alpha} & -v_{n,\alpha} \\ v_{n,\alpha} & u_{n,\alpha} \end{pmatrix} \begin{pmatrix} b_{\alpha,n,\uparrow} \\ b_{\alpha,n,\downarrow}^\dagger \end{pmatrix}, \tag{B4}$$

to obtain the desired Hamiltonian $H_{\text{And}}^{\text{sc}}$ in Eq. (13). The matrix elements are determined by

$$u_{n,\alpha}^2 - v_{n,\alpha}^2 = \frac{V_n^{\alpha 2} - W_n^{\alpha 2}}{V_n^{\alpha 2} + W_n^{\alpha 2}}, \quad u_{n,\alpha} v_{n,\alpha} = \frac{-V_n^\alpha W_n^\alpha}{V_n^{\alpha 2} + W_n^{\alpha 2}}. \tag{B5}$$

The parameters $\xi_n^\alpha, \gamma_n^\alpha, \delta_n^\alpha$ in Eq. (13) are related to the ones in H_{AFM} by

$$\xi_n^\alpha = (u_{n,\alpha}^2 - v_{n,\alpha}^2) L_n^\alpha, \quad \gamma_n^\alpha = \sqrt{V_n^{\alpha 2} + W_n^{\alpha 2}}, \tag{B6}$$

$$\delta_n^\alpha = -u_{n,\alpha} v_{n,\alpha} L_n^\alpha. \tag{B7}$$

We compared the numerical values obtained from the procedure described in Sec. III for the SC case with the ones from earlier AFM calculations for half filling using the above relations. A reasonable agreement for the two different calculations was found.

[1] C. J. Halboth and W. Metzner, Phys. Rev. Lett. **85**, 5162 (2000).
[2] D. Zanchi and H. J. Schulz, Phys. Rev. B **61**, 13609 (2000).
[3] C. Honerkamp, M. Salmhofer, N. Furukawa, and T. M. Rice, Phys. Rev. B **63**, 035109 (2001).
[4] M. Aichhorn, E. Arrigoni, M. Potthoff, and W. Hanke, Phys. Rev. B **74**, 024508 (2006).
[5] R. Micnas, J. Ranninger, and S. Robaszkiewicz, Rev. Mod. Phys. **62**, 113 (1990).
[6] J. Bardeen, L. Cooper, and J. Schrieffer, Phys. Rev. **108**, 1175 (1957).
[7] I. Bloch, J. Dalibard, and W. Zwerger, Rev. Mod. Phys. **80**, 885 (2008).
[8] M. Greiner, C. Regal, and D. Jin, Nature (London) **426**, 537 (2003).
[9] M. W. Zwierlein, C. A. Stan, C. H. Schunck, S. M. F. Raupach, A. J. Kerman, and W. Ketterle, Phys. Rev. Lett. **92**, 120403 (2004).
[10] M. Zwierlein, J. Abo-Shaeer, A. Shirotzek, C. H. Schunck, and W. Ketterle, Nature (London) **435**, 1047 (2005).
[11] J. K. Chin, D. E. Miller, Y. Liu, C. Stan, W. Setiawan, C. Sanner, K. Xu, and W. Ketterle, Nature (London) **443**, 961 (2006).
[12] D. M. Eagles, Phys. Rev. **186**, 456 (1969).
[13] A. J. Leggett, in *Modern Trends in the Theory of Condensed Matter*, edited by A. Pekalski and R. Przystawa (Springer, Berlin, 1980).
[14] P. Nozières and S. Schmitt-Rink, J. Low Temp. Phys. **59**, 195 (1985).
[15] M. Randeria, in *Bose-Einstein Condensation*, edited by A. Griffin, D. Snoke, and S. Strinagari (Cambridge University Press, Cambridge, England, 1995).
[16] A. Toschi, M. Capone, and C. Castellani, Phys. Rev. B **72**, 235118 (2005).
[17] Q. Chen, K. Levin, and J. Stajic, J. Low Temp. Phys. **32**, 406 (2006).
[18] N. Dupuis, Phys. Rev. B **70**, 134502 (2004).
[19] K. Wilson, Rev. Mod. Phys. **47**, 773 (1975).
[20] R. Bulla, T. Costi, and T. Pruschke, Rev. Mod. Phys. **80**, 395 (2008).
[21] R. Peters, T. Pruschke, and F. B. Anders, Phys. Rev. B **74**, 245114 (2006).
[22] A. Weichselbaum and J. von Delft, Phys. Rev. Lett. **99**, 076402 (2007).
[23] F. B. Anders and A. Schiller, Phys. Rev. Lett. **95**, 196801 (2005).
[24] J. Bauer and A. C. Hewson, Europhys. Lett. **85**, 27001 (2009).
[25] M. Keller, W. Metzner, and U. Schollwöck, Phys. Rev. Lett. **86**, 4612 (2001).
[26] M. Capone, C. Castellani, and M. Grilli, Phys. Rev. Lett. **88**, 126403 (2002).
[27] A. Garg, H. R. Krishnamurthy, and M. Randeria, Phys. Rev. B **72**, 024517 (2005).
[28] A. Toschi, P. Barone, M. Capone, and C. Castellani, New J. Phys. **7**, 7 (2005).
[29] B. Kyung, A. Georges, and A.-M. S. Tremblay, Phys. Rev. B **74**, 024501 (2006).
[30] A. Georges, G. Kotliar, W. Krauth, and M. Rozenberg, Rev. Mod. Phys. **68**, 13 (1996).
[31] W. Metzner and D. Vollhardt, Phys. Rev. Lett. **62**, 324 (1989).
[32] K. Satori, H. Shiba, O. Sakai, and Y. Shimizu, J. Phys. Soc. Jpn. **61**, 3239 (1992).
[33] O. Sakai, Y. Shimizu, H. Shiba, and K. Satori, J. Phys. Soc. Jpn. **62**, 3181 (1993).
[34] T. Yoshioka and Y. Ohashi, J. Phys. Soc. Jpn. **69**, 1812 (2000).
[35] M.-S. Choi, M. Lee, K. Kang, and W. Belzig, Phys. Rev. B **70**, 020502(R) (2004).
[36] A. Oguri, Y. Tanaka, and A. C. Hewson, J. Phys. Soc. Jpn. **73**, 2494 (2004).
[37] J. Bauer, A. Oguri, and A. Hewson, J. Phys.: Condens. Matter **19**, 486211 (2007).
[38] T. Hecht, A. Weichselbaum, J. von Delft, and R. Bulla, J. Phys.: Condens. Matter **20**, 275213 (2008).
[39] R. Bulla, T. Pruschke, and A. C. Hewson, J. Phys.: Condens. Matter **9**, 10463 (1997).
[40] R. Zitzler, T. Pruschke, and R. Bulla, Eur. Phys. J. B **27**, 473 (2002).
[41] J. Bauer and A. C. Hewson, Eur. Phys. J. B **57**, 235 (2007).
[42] R. Bulla, Phys. Rev. Lett. **83**, 136 (1999).
[43] G. Sangiovanni *et al.*, Phys. Rev. B **73**, 205121 (2006).
[44] A. Martin-Rodero and F. Flores, Phys. Rev. B **45**, 13008 (1992).
[45] C. A. Regal, M. Greiner, S. Giorgini, M. Holland, and D. S. Jin, Phys. Rev. Lett. **95**, 250404 (2005).
[46] T. Pruschke, D. L. Cox, and M. Jarrell, Phys. Rev. B **47**, 3553 (1993).
[47] These results are robust with respect to broadening as the excitation can be seen directly in the raw data.
[48] P. Pieri, L. Pisani, and G. C. Strinati, Phys. Rev. B **70**, 094508 (2004).
[49] A feature of the infinite-dimensional model is that it does not include a collective Goldstone mode. A coupling of the fermions to the Goldstone mode in a more general model can lead to a damping of low-energy quasiparticles.
[50] K. Borejsza and N. Dupuis, Europhys. Lett. **63**, 722 (2003).
[51] K. Borejsza and N. Dupuis, Phys. Rev. B **69**, 085119 (2004).
[52] R. Bulla, A. C. Hewson, and T. Pruschke, J. Phys.: Condens. Matter **10**, 8365 (1998).